1998-09

Observations and Analysis of the 10-11 June 1994 Coastally Trapped Disturbance

Ralph, F.M.; Armi, L.; Bane, J.M.; Dorman, C.; Neff, W.D.; Neiman, P.J.; Nuss, W.; Persson, P.O.G.

Monthly Weather Review, Volume 126, pp. 2435-2465, 1998.
http://hdl.handle.net/10945/44300

Observations and Analysis of the 10–11 June 1994 Coastally Trapped Disturbance

F. M. RALPH,* L. ARMI,+ J. M. BANE,# C. DORMAN,+ W. D. NEFF,* P. J. NEIMAN,* W. NUSS,@ AND P. O. G. PERSSON&

* *NOAA/ERL/Environmental Technology Laboratory, Boulder, Colorado*
+ *Scripps Institution of Oceanography, La Jolla, California*
# *Marine Sciences Program, University of North Carolina, Chapel Hill, North Carolina*
@ *Department of Meteorology, Naval Postgraduate School, Monterey, California*
& *CIRES/NOAA, University of Colorado, Boulder, Colorado*

(Manuscript received 23 January 1997, in final form 13 November 1997)

ABSTRACT

A coastally trapped disturbance (CTD), characterized by southerly flow at the surface on 10–11 June 1994, was observed from the California Bight to Bodega Bay during a field experiment along the California coast. (North–south approximates the coast-parallel direction.) Data from a special observational network of wind profilers, radio acoustic sounding systems, special surface data, balloon ascents, and a research aircraft were used with satellite and synoptic data to explore both the CTD structure and the regional-scale changes before the event.

The disruption of the climatological northerly flow along the central California coast, which preconditioned the area for the development of a CTD, began with the eastward movement of a surface high into Washington and Oregon and the amplification of a thermal low in northern California. As with most CTDs in the region, this occurred over the 2–3 days preceding the CTD's initiation. These large-scale changes caused westward advection of warm continental air across much of the California coast, which increased temperatures by 10°–12°C in the layer from 0.4 to 2.0 km above mean sea level (MSL) during the 48 h before southerly flow appeared offshore at the surface. The warming reversed the alongshore sea level pressure gradients near the coast by creating a region of pressure falls extending along 600–1000 km of the coast. This also modified the cross-shore pressure gradient and thus the geostrophic alongshore flow. The warming along the coast also increased the strength of the temperature inversion capping the marine boundary layer (MBL) by a factor of 2–4 over 48 h. The synoptic-scale changes also moved the axis of the climatological near-surface, northerly jet much farther offshore from central California and strengthened this jet near the headlands of Capes Mendocino and Blanco.

The development and decay of southerly flow at the surface along the coast coincided roughly with the evolution of a mesoscale low 200 km offshore, and of a coastal ridge roughly 100 km wide. However, the CTD initiation also followed a 500-m thickening of the MBL inversion in the California Bight region where a Catalina eddy was initially present. At surface sites, the CTD was marked by the passage of a pressure trough, followed by a gradual shift to southerly flow and the appearance of clouds. The area of low cloud was not coincident with the region of southerly flow. The transition to southerly flow propagated northward along shore at 11.9 $\pm$ 0.3 m s^{-1} on 10 June, stalled for 11–12 h during the part of the diurnal cycle normally characterized by enhanced northerly flow, and then continued propagating northward along shore at 11.6 m s^{-1}. Both the geostrophic wind and the isallobaric component of the ageostrophic wind were consistent with southerly flow at the surface. Southerly flow was observed up to 5 km MSL in this event and in others, which indicates that the synoptic-scale environment of many CTDs in this region may include a deep tropospheric cyclonic circulation or trough offshore.

Both cross-shore and alongshore flights performed by a research aircraft documented the CTD structure and showed that the southerly flow extended at least 100 km offshore and appeared first within the MBL inversion as the inversion thickened upward. While the top of the inversion rose, the height of the inversion's base remained almost unchanged. The thickening of the inversion decreased with distance offshore, and there was no significant change in the MBL depth (i.e., the inversion base height), until 12–14 h after the surface wind shift. Thus, it is suggested that two-layer, shallow water idealizations may be unable to represent this phenomenon adequately. Nonetheless, the gradual wind shift, the thickening inversion, and the correlation between southerly flow and a mesoscale coastal pressure ridge are consistent with a coastally trapped Kelvin wave, albeit one with a higher-order vertical structure that can exist in a two-layer model. However, the semipermanent nature of the changes in the MBL and its inversion is more characteristic of a shallowly sloped internal bore. The temperature increase and lack of southerly flow exceeding the northward phase speed are inconsistent with gravity current behavior.

Corresponding author address: Dr. F. Martin Ralph, NOAA/ERL/ETL, Mail Code R/E/ET7, 325 Broadway, Boulder, CO 80303.
E-mail: fralph@etl.noaa.gov

1. Introduction

Although the average wind flow along the United States west coast during summer is northerly to northwesterly, it is interrupted several times each year by episodes of southerly or southeasterly flow that are not associated with land-falling, synoptic-scale baroclinic systems, that is, fronts or troughs (Bond et al. 1996). The transitions from northerly to southerly flow are often marked by the onset of low clouds and fog that can significantly affect coastal and maritime activity (e.g., Leipper 1995) and can modify regional air pollution distributions. While the wind transitions at a particular site are usually rather gradual (e.g., 8 m s^{-1} change in alongshore wind over 4–10 h; Bond et al. 1996), occasionally the transitions are abrupt, and the southerlies can reach 15 m s^{-1} within a few minutes (Mass and Albright 1987).

The earliest study to document this phenomenon along the United States west coast (Dorman 1985) found that the region of southerlies propagated northward and appeared to have the structure of a coastally trapped solitary Kelvin wave. Gill (1977) had earlier identified similar disturbances along the African coast, and suggested that they were analogous to coastally trapped Kelvin waves found in the ocean (e.g., Miles 1972; Gill 1982; Maxworthy 1983). Such a wave in the atmosphere consists of a region of elevated marine boundary layer (MBL) beneath which the flow is southerly (Gill 1982; Beardsley et al. 1987). The disturbance is trapped along coastal mountains by Coriolis effects, propagates parallel to the mountains, and is expected to decay exponentially offshore, within approximately 100 km (i.e., the Rossby radius of deformation). Through other case studies it was recognized that the transitions to southerly flow sometimes more closely resembled a density current (Mass and Albright 1987; Dorman 1987; Hermann et al. 1990)—that is, the transitions were more abrupt, were associated with rapid cooling and its associated pressure increase, and propagated at a speed characteristic of density currents. It has also been shown that the southerly flow develops when synoptic forcing changes the alongshore pressure gradient from its normal condition into one with lower pressures to the north. Under this condition, it has been suggested that ageostrophic southerly flow develops because of the blocking effect of the coastal mountain ranges (Mass and Albright 1987). More recently, Reason and Steyn (1992) presented a ''unifying theory'' based on the hypothesis that the initial perturbation of the MBL could evolve over 1–2 days into a solitary Kelvin wave with a sharp leading edge. The synoptic-scale forcing that initially perturbs the MBL, as is described in Mass and Bond (1996), involves the movement of a deep-tropospheric ridge into the Pacific Northwest and southwestern Canada resulting in a coastal extension of the trough usually located over the interior of central and southern California. It has also been suggested that flow toward the coast in the south could help perturb the MBL (Dorman 1985). The importance of these synoptic-scale factors is supported by recent analyses using a simplified model (Rogerson and Samelson 1995; Samelson and Rogerson 1996) in which a deep, closed low approaching the coast is shown to generate a coastally trapped Kelvin wave that may propagate unsteadily northward. This paper will use the term coastally trapped disturbance (CTD) to refer to these complex events, which are characteristically trapped near the coast, represent an anomaly from the seasonal mean, and include several important components beyond just the wind reversal (i.e., perturbations to pressure, changes of the MBL and its capping inversion, and the development of fog).

Based on a 10-yr climatology using 73 CTDs it was found that strong CTDs at buoys along the United States west coast occur one to two times per month during the summer, where strong is defined as $U > 5$ m s^{-1} at one of the buoys (Bond et al. 1996). (Here U is the alongshore wind component, and is positive when directed poleward along the coast. Thus $U > 0$ is referred to as southerly flow. Although the coast is not oriented truly north–south, the terms southerly and northerly are used here to refer to the alongshore wind component.) They propagate at an average speed of 7–8 m s^{-1}, last 24–36 h, cover 500–1000 km of coastline, and tend to be more abrupt to the north than to the south. It has also been shown that CTDs occur under relatively specific synoptic-scale conditions (Mass and Bond 1996). These include the onshore movement of a lower-tropospheric high pressure ridge into the Pacific Northwest, which creates a geostrophic easterly component in the lower-tropospheric flow south of the ridge axis. They hypothesize that a lee trough develops west of the coast ranges in response to downslope flow, creating the alongshore pressure gradient favoring ageostrophic southerly flow to the south of the easterlies aloft. Under this scenario, the northward progression of the southerly flow is simply a result of the changing synoptic-scale conditions and does not necessarily represent a wavelike perturbation of the MBL. However, the Bond et al. (1996) climatology clearly showed that the wind shifts were typically much more abrupt at the northern buoys than at the southern buoys (an 8 m s^{-1} change in alongshore wind over 1 h versus a similar change over 4–10 h). This finding is consistent with the hypothesis that a more abrupt transition can develop with time as the initial MBL perturbation propagates northward and a nonlinear Kelvin wave steepens (Reason and Steyn 1992). However, because very few CTDs move all the way up the coast, the north–south variations in the character of the transition could instead result from north–south variations in the synoptic and mesoscale environments. Recently, it has been recognized that local pressure changes due to synoptic-scale changes are likely to be much larger than those due to possible Kelvin waves, making it difficult to identify Kelvin wave pressure sig-

nals in operational data (Mass 1995; Reason and Steyn 1995).

To better understand which of these hypotheses represents the CTD phenomenon best, a field experiment was performed along the United States west coast during the summer of 1994 as part of the Coastal Meteorology Accelerated Research Initiative of the Office of Naval Research. This program was also based on the recognition that new observational techniques could be applied to this phenomenon and that CTDs represent an important class of coastal meteorological behavior for which improved understanding could potentially benefit the large population within coastal communities through improved forecasting (National Research Council 1992). Such an experiment was required partly because the standard operational 12-hourly soundings significantly undersample a disturbance that lasts 24–36 h, and no information is available offshore about atmospheric conditions above the surface, including the depth of the MBL.

This paper presents observations and analyses of a CTD that occurred on 10–11 June 1994, based on a unique and extensive experimental dataset (Fig. 1; Table 1) that substantially ameliorates these major limitations. This study focuses on the structure and evolution of both the disturbance and its environment. In terms of the key variables of U and pressure, this case closely resembles the composite of 15 CTDs observed at buoy 28 shown in Bond et al. (1996), and reproduced here in Fig. 2. However, it is somewhat stronger (6.5 m s^{-1}), and qualifies as ''strong'' using the criterion in Bond et al. (1996) that the southerly flow exceeds 5 m s^{-1}. Table 2 summarizes this comparison, and establishes the similarity of their key timescales, based on the major alongshore wind shift (13 and 15 h), and the time between minimum and maximum pressure (37 and 30 h). This comparison establishes that the 10–11 June 1994 CTD studied here is representative of most strong cases along the California coast. Other papers also explore this event, but emphasize other aspects of the CTD phenomenon: Thompson et al. (1997) study the relationship between the CTD and the effects of coastal mountains on blocking, downslope flow, and the sea breeze; Dorman et al. (1998) investigate the stratus cloud formation in the surface mixed layer; and Persson et al. (1996) explore the relationship between the CTD and potential vorticity anomalies frictionally generated by strong northerly flow along the steep coastal mountains.

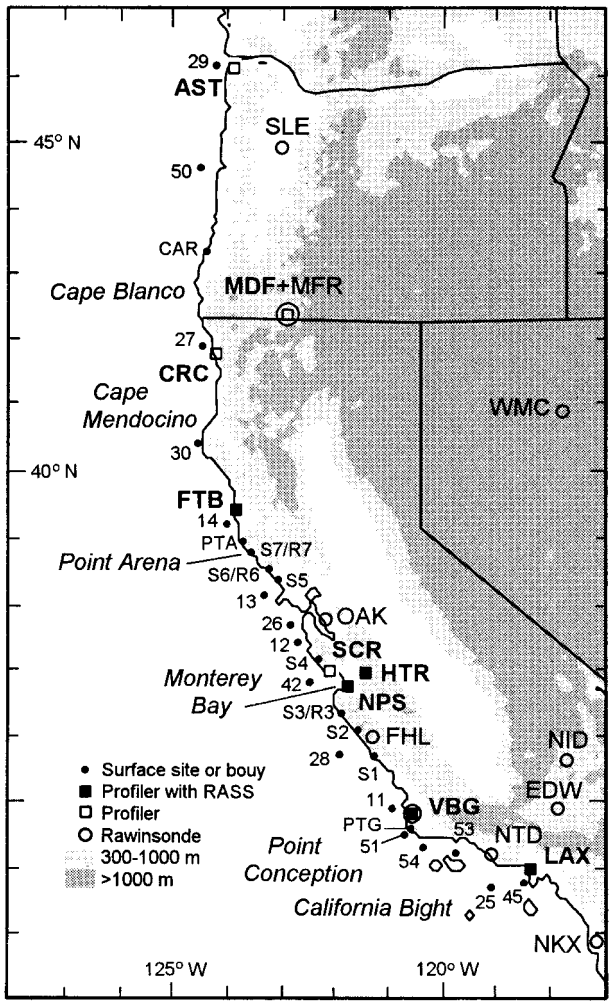

FIG. 1. Base map showing key operational and experimental observing sites and terrain features for the coastal meteorology experiment during the summer of 1994. Buoy numbers *xx* used here all represent buoys numbered 460*xx* by NDBC.

2. Experimental setup

Locations of the key observing systems used in this study are shown in Fig. 1, and their characteristics are summarized in Table 1. Nine radar wind profilers were sited along 1400 km of the west coast from Los Angeles, California, to Astoria, Oregon (Fig. 1), at an average spacing of about 200 km. These instruments are ground-based radars that provide hourly vertical profiles of horizontal wind with roughly 100–250-m vertical spacing in clear, cloudy, and precipitating conditions (Strauch et al. 1987; Ecklund et al. 1988; Ralph et al. 1995). Hourly, consensus-averaged winds, which are used here, were calculated from measurements made every 1–6 min. The hourly winds were edited using the continuity method of Weber et al. (1993). Some limited intervals of interference from migrating birds were removed using the techniques described by Wilczak et al. (1995). When combined with an acoustic source, such a radar can be used to measure the speed of sound as a function of height and is referred to as a radio acoustic sounding system (RASS) (May et al. 1989). Vertical profiles of virtual temperature (T_v) can then be calculated from the relationship between the speed of sound and T_v, and then transformed into virtual potential temperature (θ_v) using the method described by Neiman et al. (1992).

TABLE 1. Instrument characteristics and locations for the 1994 experiment on coastally trapped disturbances in California.

Instrument	Site name	Lat (°N)	Long (°W)	Altitude MSL (m)	Variables measured	Temporal sampling	Height range MSL (km)	Height resolution (m)
Aircraft	Piper Seneca III	—	—	—	*P, T, q, U, V*	1 s	0.06–2.5	Variable
Profiler†/	Vandenberg (VBG)	34.77	120.53	149	*U, V*	1 h	0.40–16.4	250–1000
RASS					T_v	1 h	0.40–3.9	250
Profiler/	Los Angeles Airport	33.94	118.44	47	*U, V*	1 h	0.15–2.0	98
RASS	(LAX)				T_v	1 h	0.17–1.4	60
Profiler*/	Naval Postgraduate School	36.69	121.76	51	*U, V*	1 h	0.14–4.0	56
RASS	(NPS)				T_v	1 h	0.15–1.5	105
Profiler*/	Hollister (HTR)	36.92	121.40	55	*U, V*	1 h	0.18–2.0	101
RASS					T_v	1 h	0.18–1.5	105
Profiler*/	Fort Bragg (FTB)	39.44	123.81	10	*U, V*	1 h	0.24–2.0	99
RASS					T_v	1 h	0.26–1.5	105
Profiler*	Santa Cruz (SCR)	36.95	122.06	12	*U, V*	1 h	0.14–2.0	101
Profiler*	Crescent City (CRC)	41.78	124.24	15	*U, V*	1 h	0.14–2.0	101
Profiler	Medford, OR (MDF)	42.37	122.87	400	*U, V*	1 h	0.52–2.5	101
Profiler	Astoria, OR (AST)	46.16	123.88	3	*U, V*	1 h	0.15–2.0	101
Radiosonde	Fort Hunter Ligget (FHL)	35.98	121.23	317	*P, T, q, U, V*	12 h	—	—
Radiosonde	Naval Postgraduate School	36.60	121.90	30	*P, T, q, U, V*	12 h	—	—
Radiosonde	*Glorita* (ship)	—	—	0	*P, T, q, U, V*	3 h	—	—
Surface station	Piedras Blancas (S1)	35.67	121.28	7	*P, T, q, U, V*	1 min	—	—
Surface station	Big Creek (S2)	36.07	121.59	60	*P, T, q, U, V*	1 min	—	—
Surface station	Point Sur North (S3)	36.32	121.88	10	*P, T, q, U, V*	1 min	—	—
Surface station	Pico Blanco (R3)	36.30	121.80	820	*P, T, q, U, V*	1 min	—	—
Surface station	Anno Nuevo (S4)	37.12	122.32	12	*P, T, q, U, V*	1 min	—	—
Surface station	Bodega Bay (S5)	38.32	123.07	9	*P, T, q, U, V*	5 min	—	—
Surface station	Fort Ross Coast (S6)	38.52	123.25	25	*P, T, q, U, V*	1 min	—	—
Surface station	Fort Ross Ridge (R6)	38.53	123.22	470	*P, T, q, U, V*	1 min	—	—
Surface station	Gualala Coast (S7)	38.80	123.56	15	*P, T, q*	1 min	—	—
Surface station	Gualala Ridge (R7)	38.90	123.70	232	*P, T, q, U, V*	1 min	—	—

* Includes a surface station; †404-MHz profiler of the National Profiler Network. All other profilers are 915 MHz. Variables measured include: pressure (*P*), temperature (*T*), virtual temperature (T_v), moisture (*q*), and south (*U*) and west (*V*) wind components.

Five of the profiler sites included RASS measurements (Fig. 1, Table 1).

An instrumented Piper aircraft (Bane et al. 1995) that could fly 1400 km over several hours, refuel, and follow the CTD northward documented the offshore structure. Temperature, relative humidity, pressure, radar altitude, and winds were measured with roughly 1-s sampling. The flexibility, range, and low cost of this aircraft made it ideal for obtaining observations in and above the MBL offshore, although the low cloud bases within the CTD precluded observing the lowest 100 m above sea level (mean sea level, MSL) in the cloudy areas. The usefulness of a small aircraft in measuring the MBL in California is illustrated by an earlier study (Edinger 1963) that documented how convective heating affects the intersection of the MBL with coastal mountains.

Along the California coast, 11 automated surface observing sites deployed for the experiment recorded data continuously at 1–5-min intervals, while 14 buoys and 2 coastal sites from the National Data Buoy Center (NDBC) provided measurements from 10 to 40 km offshore on an hourly basis (Fig. 1, Table 1). Buoy numbers *xx* used here all represent buoys numbered 460*xx* by NDBC. In addition, the Monterey Area Ship Tracks experiment was performed during June and provided a complementary dataset including surface and sounding data from the ship *Glorita*, which was in and near Monterey Bay during the CTD.

3. Synoptic conditions

a. Climatology and key geophysical features along the United States west coast

During summer, the coastal zone of the western United States is strongly affected by the East Pacific high in the lower troposphere normally centered roughly 2000–2500 km west of California near 40°N (Neiburger et al. 1961; Beardsley et al. 1987; Mass and Bond 1996). This high produces northerly or northwesterly flow along the West Coast that contributes strongly to upwelling of cold ocean waters near shore (e.g., Nelson 1977; Beardsley et al. 1987), which cools the boundary layer air above it to <15°C along much of the coast north of Point Conception. This contrasts with inland deserts and grasslands, where temperatures often reach 40°C and oscillate diurnally by 15°C within 100 km of the coast, helping to create pronounced land–sea-breeze (e.g., Banta 1995) and mountain–valley (e.g., Whiteman 1990) circulations. The combination of large-scale subsidence associated with the synoptic-scale East Pacific high (Neiburger et al. 1961), cold sea surface temper-

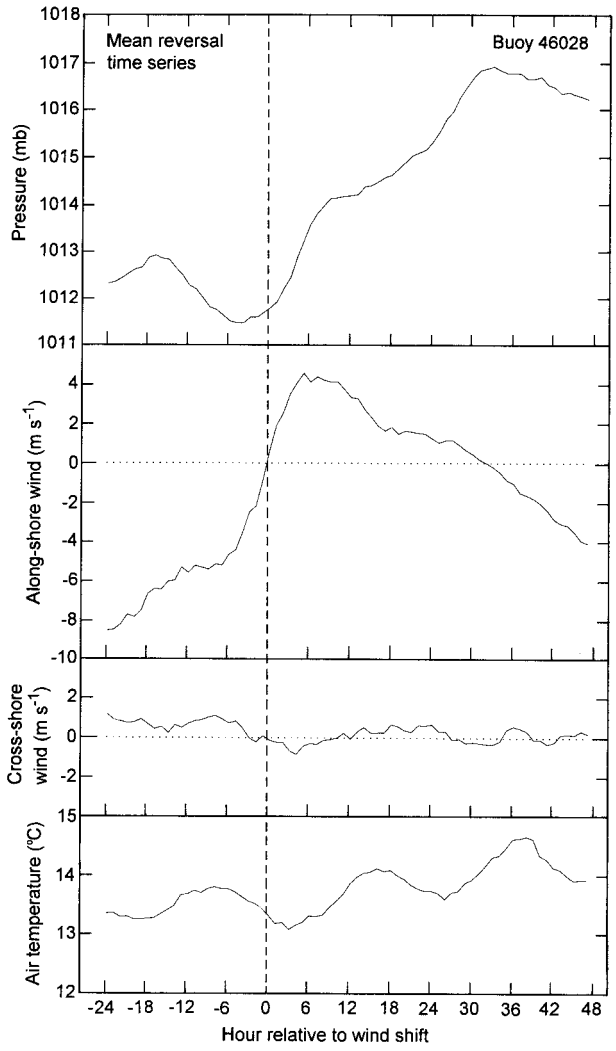

FIG. 2. Time series showing observed changes at buoy 28 associated with CTDs. The curves represent a composite of 15 CTDs observed at that buoy. The times represent hours relative to the time of the shift from northerly to southerly flow. Strong perturbations in pressure and alongshore wind are evident (from Bond et al. 1996.) The time axis was adjusted slightly from that in Bond et al. (1996) so that the alongshore wind speed and time = 0 are perfectly aligned.

atures due to upwelling, a nearby source of extremely hot air, and coastal mountains creates a strong temperature inversion of roughly 10°C separating the warm free troposphere above from the cool MBL below. A climatology of the MBL and its capping inversion was performed by Neiburger et al. (1961) using more than 6000 soundings from June to September along the California coast. Their results indicate that the MBL during these months is usually 400 m deep along the central and northern California coasts and rises offshore to roughly 2000 m over Hawaii, and that the inversion itself is typically 600 m thick. Transient, synoptic-scale weather systems modulate the height and strength of the MBL's capping inversion through their vertical motions and horizontal thermal advections.

TABLE 2. Comparison of the 10–11 June 1994 CTD as observed at buoy 46028 with the composite of 15 other CTDs also at buoy 46028 (from Bond et al. 1996).

Parameter	Composite of 15 events	10–11 June 1994 event
Maximum southerly wind	4.6 m s^{-1}	6.5 m s^{-1}
Maximum northerly wind roughly 12 h before shift to southerly	5.5 m s^{-1}	7.7 m s^{-1}
Time required for major wind shift	13 h	15 h
Maximum pressure difference from 24 h before to 48 h after wind shift	5.3 mb	5.7 mb
Time between minimum and maximum pressures	37 h	30 h

b. The synoptic environment of the 10–11 June 1994 coastally trapped disturbance

This section explores the factors that disrupted the climatological conditions along the California coast and contributed to the creation of the strong CTD on 10 June 1994. This is aided by a recent summary of synoptic conditions associated with 73 strong CTDs observed at four buoys from central California to the Columbia River between 1981 and 1991 (Mass and Bond 1996). The synoptic conditions during the 48 h before the 10–11 June 1994 CTD developed (Fig. 3) are similar to those identified in the CTD climatology for buoy 13, which is northwest of San Francisco Bay and was near the northernmost penetration of the CTD in this event [synoptic conditions for buoy 28 were not shown in Mass and Bond (1996) but are very similar to those for buoy 13]. The key features are the amplification of a transient deep-tropospheric ridge over the Pacific Northwest and the onshore movement of its associated surface high into the Pacific Northwest, as well as an amplifi-

→

FIG. 3. Synoptic conditions at the surface, 850 mb, and 500 mb. Surface station plots include wind velocities (half barb = 2.5 m s^{-1}; full barb = 5 m s^{-1}; flag = 25 m s^{-1}), temperature (°C; upper left), dewpoint temperature (°C; lower left), and sea level pressure (mb; lower right). Upper-level station plots are the same except that geopotential height is shown (m; lower right). Automated sea level pressure analyses (solid; contoured every 4 mb) are shown on surface charts. Automated geopotential height analyses (solid; contoured every 15 and 60 m, at 850 and 500 mb, respectively) and temperature analyses (dashed; contoured every 2°C) are shown at upper levels. These analyses are from a data assimilation technique using multiquadric interpolation (Nuss and Titley 1994) at each analysis time, which includes the experimental data and NCEP's Eta Model first-guess fields over the ocean.

1200 UTC 8 Jun 94

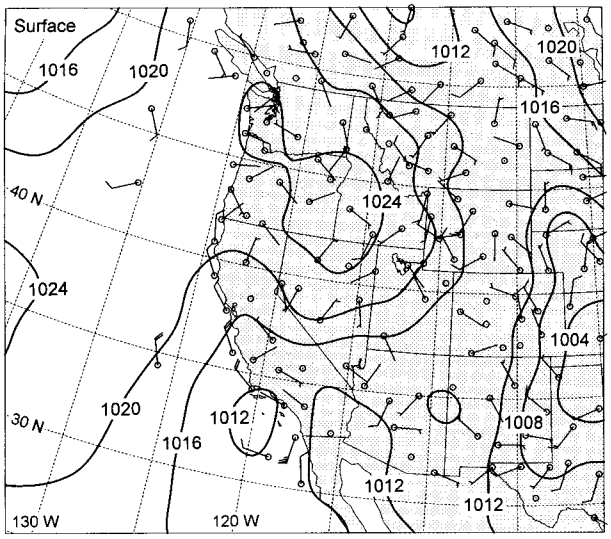

1200 UTC 9 Jun 94

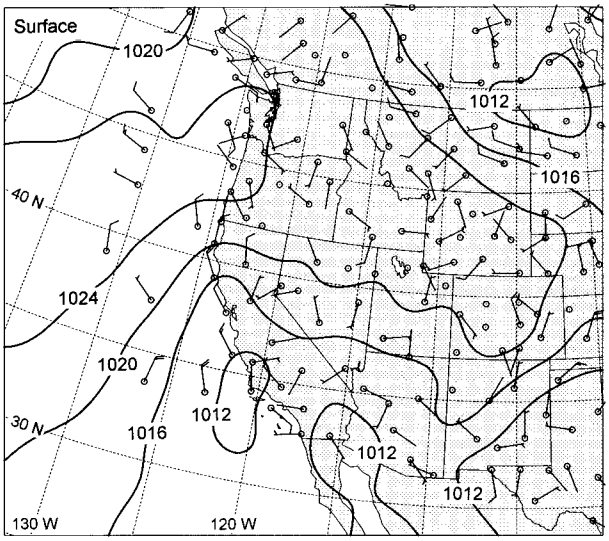

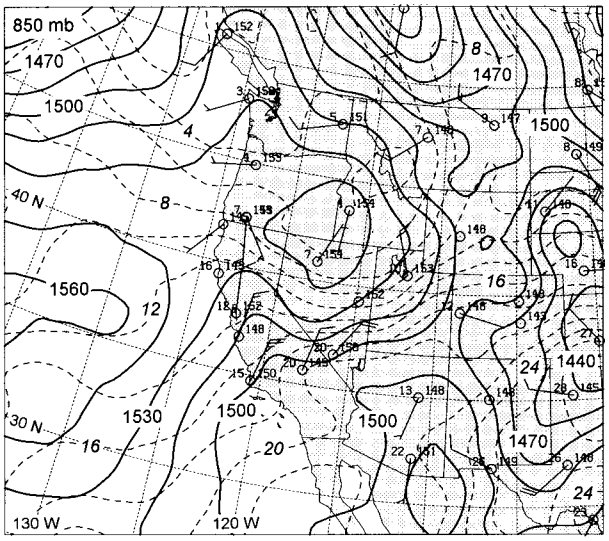

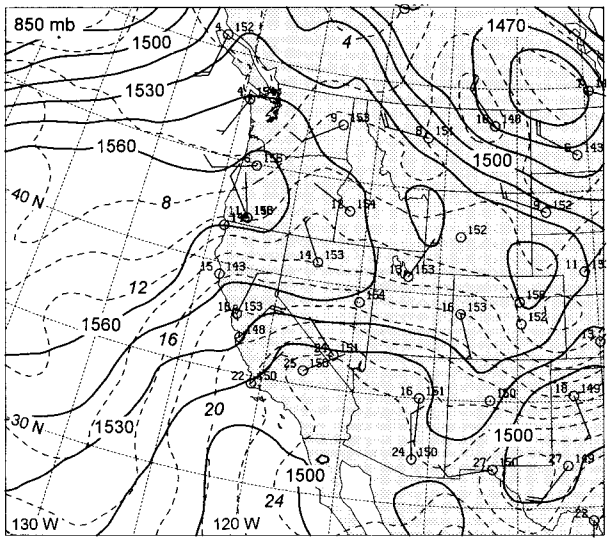

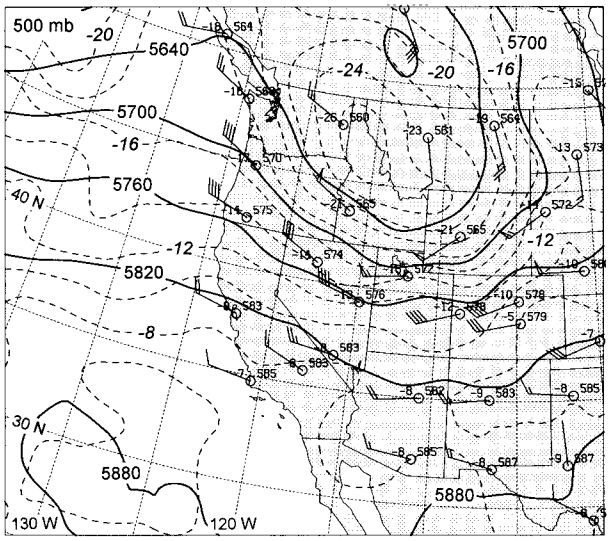

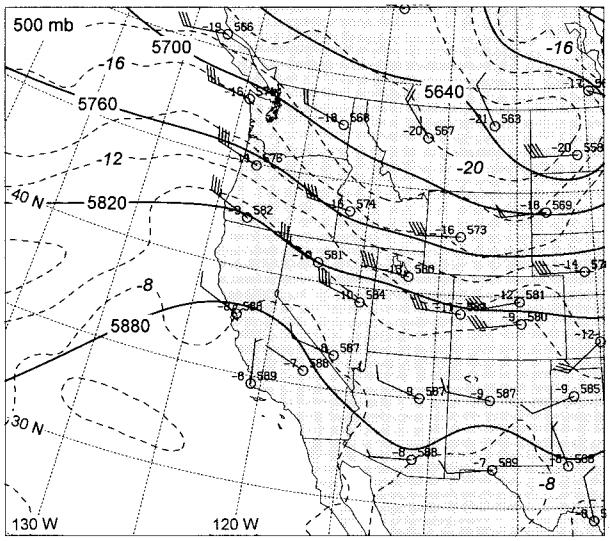

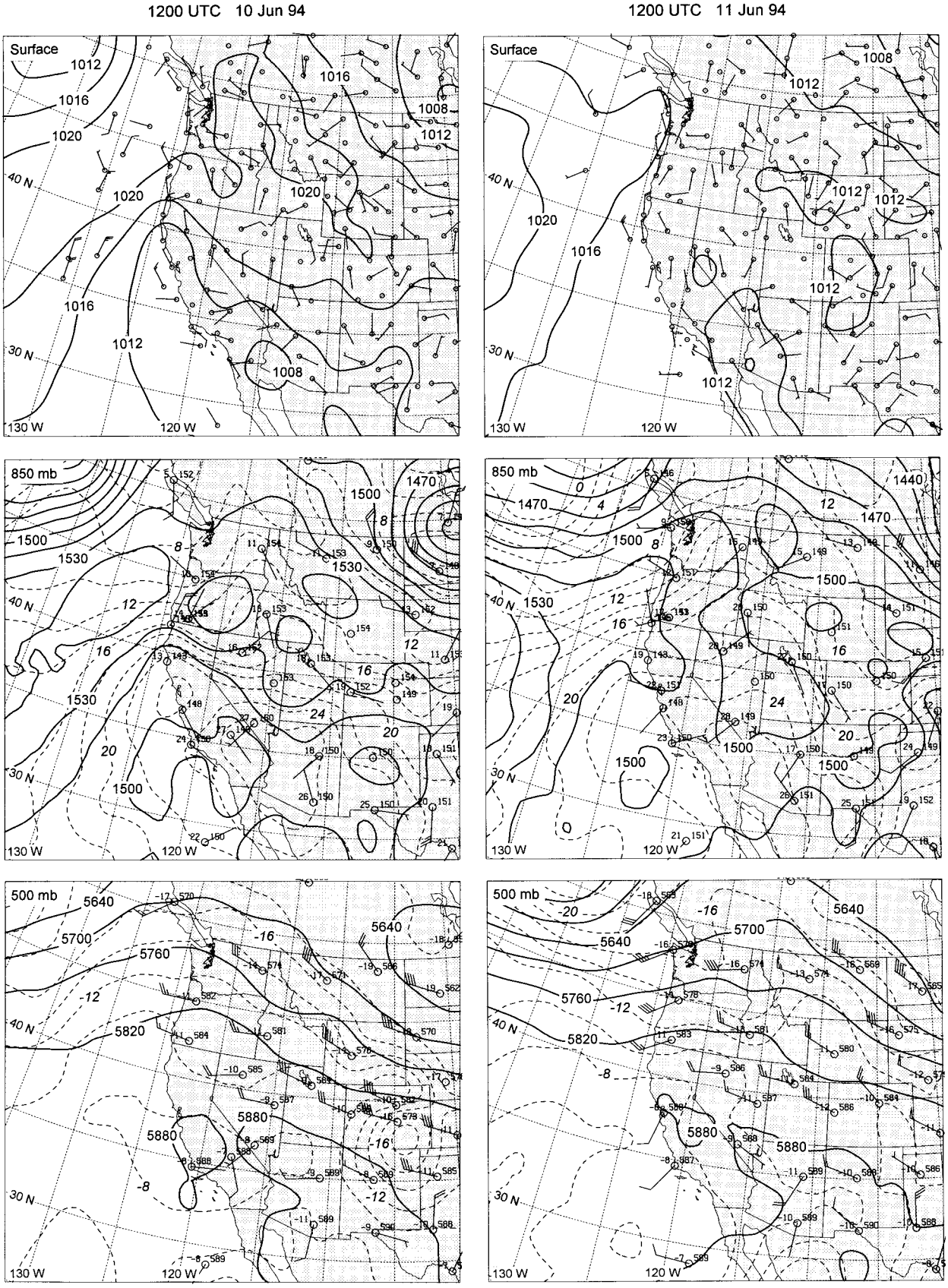

FIG. 3. (*Continued*)

cation and northward development of a thermally induced sea level pressure trough (a thermal trough) over northern California (Figs. 3 and 4). The northward-directed, alongshore pressure gradient increased from 4.8 mb/1000 km at 0000 UTC 9 June to 8.0 mb/1000 km at 0000 UTC 10 June as the center of this region of strong gradient was displaced northward from near Monterey Bay to the California–Oregon border (Figs. 4a and 4d). Simultaneously, the alongshore pressure gradient along the central California coast decreased from 4.8 mb/1000 km to near zero (Figs. 3, 4a, and 4d).

Conditions did differ from the Mass and Bond (1996) climatology in some respects. The 500-mb ridge was weaker and amplified less than in the climatology [a 150-km increase in the northward displacement of a geopotential height contour during 48 h in this case (Fig. 3) vs a 450-km displacement in the climatology]. The surface high moved into the Pacific Northwest roughly 72 h before the CTD started, rather than 48 h before, and did not amplify significantly. The thermal trough over California developed more than in the climatology, as indicated by 48-h pressure falls of 5–8 mb in northern California in this case (Figs. 4b and 4e), compared to 2–3 mb in the climatology. These two differences offset one another in terms of changing the alongshore pressure gradient along the northern California coast, which increased by approximately 65% over 48 h in the 10–11 June 1994 event and in the climatology. Also, although the pressure gradient favored flow with a strong geostrophic easterly wind component and possible lee troughing near the Oregon–California border, which is seen in the climatology as well, wind profilers in the area observed no clear easterly wind component up to 3 km MSL during this period (not shown). However, easterly flow was present over the central California coast south of this region of strong alongshore pressure gradient.

Sea level pressure changes over the two 24-h periods before the CTD developed were calculated hydrostatically from the standard rawinsonde network for the layer from the surface to 2 km MSL (Figs. 4c and 4f). Because some sites are in the mountains, the layer between the surface and 2 km MSL was artificially thin, and thus biased the hydrostatic pressure changes calculated from the ground to 2 km MSL toward lower values. Even though several stations that are near or above 2 km MSL were excluded from this analysis, this error contributed to the broad minimum in calculated pressure changes over the intermountain region. Nonetheless, the data are still adequate to reveal overall patterns, and the coastal regions are not affected. The analyses in Fig. 4 indicate that a broad region of warming caused pressure falls over and west of the intermountain region, with the greatest changes located along the California coast west of the Sierra Nevada mountains. The correlation between the observed and calculated pressure falls shows that warming in the lowest 2 km MSL was primarily responsible for changing the alongshore, and cross-shore sea level pressure field, but that some influence from higher levels was also present, especially over northern California and Oregon. The region of significant pressure falls (>2 mb in 24 h) covered roughly 600–1000 km of coastline, and its center moved northward from near Monterey Bay to the California–Oregon border over 24 h. Near the center of this broader-scale region, there is a smaller, mesoscale region of enhanced pressure falls of an additional 1–2 mb/24 h that covered roughly 300 km of coastline and extended roughly 150–200 km inland. Because the lower-tropospheric warming and sea level pressure falls had a local maximum along the coast, they modified the initial climatological northward pressure gradient in a way that decreased (increased) the alongshore pressure gradient to the south (north) of the pressure-fall center. This acted to precondition the coastal environment for the development of southeasterly flow by weakening or removing both the alongshore pressure gradient supporting the strong ageostrophic northwesterly flow characteristic of the region and the cross-shore pressure gradient supporting the geostrophic component of the northerly flow (Figs. 3 and 4). The increased pressure gradient north of the pressure-fall maximum is also possibly involved in the generation of a CTD, as described in Persson et al. (1996). The origins of the warming that led to the preconditioning are discussed in detail in a later section, where it is shown that the warming along the central California coast resulted primarily from warm advection from the hot continental interior, rather than from downslope warming. It should also be noted that the pressure tendency fields in Figs. 4c and 4f, when compared to the sea level pressure fields, indicate that the cross-shore pressure gradient is also affected. Considered in the context of the synoptic-scale westward increase in pressure across the coast, the pressure tendencies act to reduce the cross-shore pressure gradient east of the center of falling pressure (and thus to decrease the geostrophic northerly winds), and to increase the cross-shore pressure gradient west of its center. Because buoys offshore tended to experience slightly greater pressure falls than the onshore sites (e.g., -6.9 mb day^{-1} vs -4.4 and -4.7 mb day^{-1}; Fig. 4e) near the pressure fall maximum, it appears that the center of pressure falls was slightly offshore.

An important difference from the Mass and Bond (1996) climatology is that the June 1994 case included a weak deep-tropospheric cyclonic circulation, or trough, west of southern and central California, as inferred from the southerlies that were observed up to 6 km MSL along the California coast during the CTD (Figs. 3 and 5). It is also likely that these deep southerlies were partly a response to a ridge at 500 mb that developed over Arizona and Mexico (Fig. 3). Deep southerlies associated with a CTD are not unique to this case study. They were also present in events documented by Dorman (1985) where southeasterly flow was observed at Vandenberg up to 4 km just before southerly

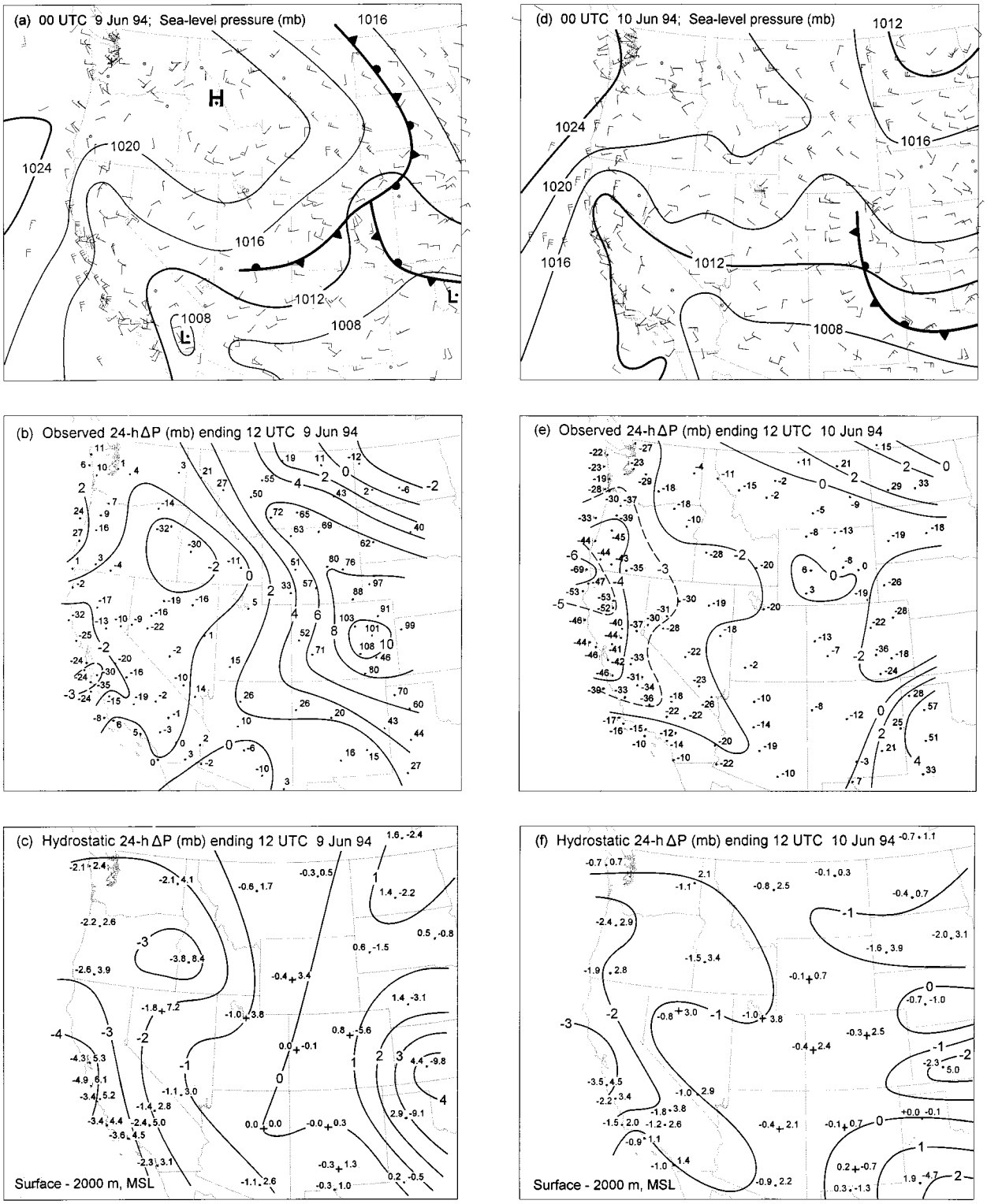

FIG. 4. (a) and (d) Surface wind vectors (as in Fig. 3), sea level pressure analysis (mb, solid), and surface fronts. (b) and (e) 24-h sea level pressure change (mb × 10), and isallobars (mb day^{-1}) drawn every 2 mb day^{-1} (solid) with intermediate isallobars also shown (dashed). (c) and (f) Hydrostatic local pressure change calculated from the layer between the surface and 2 km MSL based on 24-h temperature changes. The 24-h pressure change (mb; left), and layer-mean temperature change (°C; right) are plotted. Those sites in (c) and (f) marked with dots had hydrostatic column depths containing at least 40% of the layer between sea level and 2 km MSL. Those with + had column depths less than 40%.

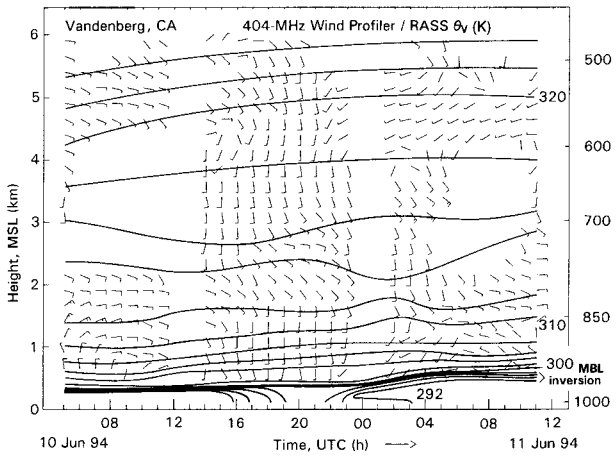

FIG. 5. Time–height section of hourly RASS and 12-hourly rawinsonde virtual potential temperature (θ_v, K, solid), and hourly consensus horizontal winds from the VBG 404-MHz radar wind profiler. Winds are as in Fig. 3. Gaps in profiler wind data are from interference due to migrating birds, and the rawinsonde ascents. The height of the MBL inversion is based on rawinsonde data at 0000 and 1200 UTC each day (0000 UTC = 1700 LST).

flow appeared at the surface, and by Mass and Albright (1987) where southerlies were observed up to at least 600 mb at San Diego and Oakland at roughly the same time southerly flow was observed at the surface offshore. Although the climatology does not show such southerlies associated with CTDs at buoys 13 and 28 along the central California coast, such a circulation was commonly associated with CTDs at the two more northern buoys [27 and 10 (note that buoy 29 replaced buoy 10)]. The reason for this difference has not been explained. It is possible, however, that the operational analyses on which the climatology was based suffered from a lack of data in the region south and southwest of southern California.

4. Perturbation evolution at the surface, northward propagation, and clouds

Because only a minimal amount of data has been available above the standard surface data used in earlier studies, CTDs have traditionally been defined by their signature at the surface and in satellite images (e.g., Dorman 1985; Bond et al. 1996). CTDs are defined primarily by a region of southerly flow that propagates poleward along shore. It usually includes a region of low cloud or fog, but this was not considered in the Bond et al. (1996) composites. This section documents the 10–11 June 1994 CTD using these traditional techniques, supplemented with experimental surface data along the coast and satellite-derived sea surface wind data offshore from the Special Sensing Microwave/Imager (SSM/I) aboard a polar-orbiting satellite (e.g., Miletta 1993). SSM/I data, which have roughly 25-km resolution, were available in the area two–four times each day from 8–12 June 1994. These data are shown at two key times (Fig. 6) to illustrate the northward and offshore displacement of a large 10–14 m s^{-1} northerly jet over 48 h.

Mesoscale analyses (Fig. 7) based on these data reveal the development of a small, low pressure center about 200 km offshore of Point Conception, which is farther south, smaller, closer to shore, and more stationary than similar mesolows analyzed by Mass and Albright (1987) in two other CTDs. As also noted by Mass and Albright (1987) in their cases, a 100-km-wide, near-shore pressure ridge developed, with pressure decreasing to the north along shore (Fig. 7). The mesolow, which represented a roughly 1–2-mb perturbation between 1800 UTC 10 June and 1800 UTC 11 June, apparently developed out of a weak trough–low that moved offshore from central California around 1200 UTC 10 June. The westward development of the initial trough is similar to the evolutions analyzed by Mass and Albright (1987) in two other events. [There was also a Catalina eddy (e.g., Mass and Albright, 1989; Clark and Dembek 1991) within the California Bight region on 10 June (Figs. 7a–d).] The analysis of this low is based largely on six reports from five ships between 1800 UTC 10 June and 1200 UTC 11 June. Because of the importance of these ship observations, their reliability was assessed by examining them at times when other buoy or ship data were present nearby. Two ships reported data of reasonable reliability, one could not be assessed, and two each had a low bias of 4.5 mb in sea level pressure. Because these bias estimates were based on multiple comparisons, they were considered reliable enough to correct the original reports. These corrected ship reports appear in Fig. 7e as 1013.4 mb south of the low, in Fig. 7f as 1014.5 mb west of the low, and in Fig. 7g as 1014.6 mb north of the low. No strong evidence of errors in wind direction or speed were evident.

The mesoscale analysis in Fig. 7e, including the mesolow, is also supported by the spatial distribution of surface wind speeds observed 6 h earlier by the SSM/I (cf. Figs. 6b and 7d). In addition to the localized minimum in wind speed roughly coincident with the position of the analyzed surface low, there is a weak southerly flow maximum of 6–7 m s^{-1} closer to shore, and two northerly flow maxima exceeding 14 m s^{-1} near Capes Mendocino and Blanco, where conclusions about the wind direction are based on nearby ship and buoy reports. Comparison between the SSM/I surface winds at 1800 UTC 10 June (Fig. 6b), and those from 24 h earlier (not shown) indicate that the minimum west of Point Conception developed between 1800 UTC 9 and 1800 UTC 10 June. Numerical simulations performed using the U.S. Navy's Coupled Oceanic and Atmospheric Mesoscale Prediction System (Hodur 1997) also contain evidence of this mesolow, although its amplitude (0.4 mb) is less than that observed (Thompson et al. 1997).

The northward expansion of this region of southerly flow is also clearly seen in Figs. 7 and 8. Southerly flow

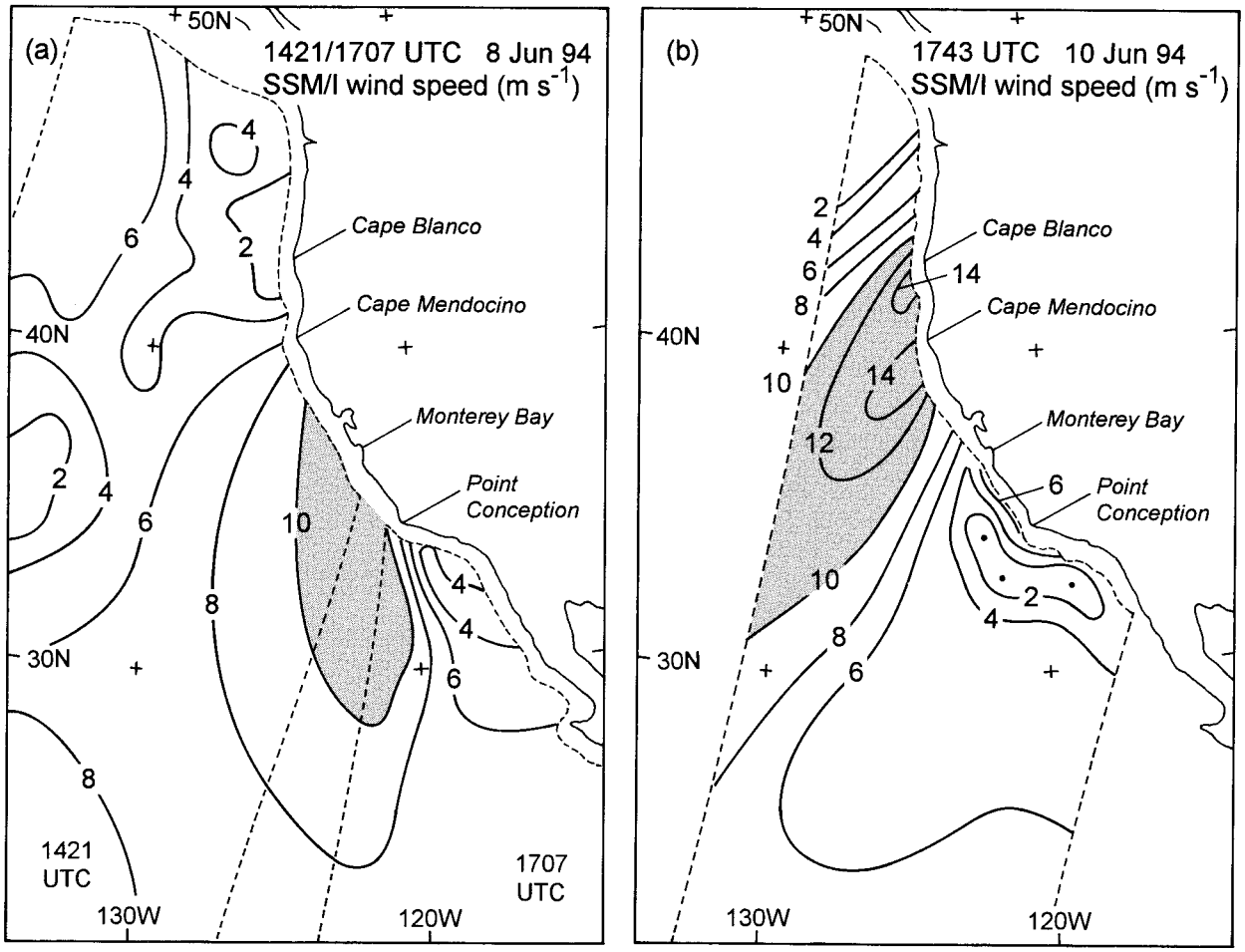

FIG. 6. SSM/I surface wind speeds (m s^{-1}) (a) before and (b) during the CTD of 10–11 June 1994.

began southeast of Point Conception between 0300 and 0600 UTC 10 June and progressed northward along shore at ~11.9 ± 0.3 m s^{-1} between 0500 and 1800 UTC 10 June, and 0600 and 1100 UTC 11 June, with a pause in between (Fig. 9). This pause corresponds to the phase of the diurnal cycle characterized by the strongest northerly flow in the MBL (Beardsley et al. 1987). (Local time along the United States west coast can be calculated by subtracting 7 h from UTC.) The uncertainty of the phase speed is based on the inclusion or exclusion of three of the buoys from the least squares best fit; buoy 25 often turns southerly during the diurnal cycle, PTGC1 is strongly affected by the headland at Point Conception, and there were two wind shifts at buoy 12. The southerly flow reached 7 m s^{-1} at some buoys but never appeared north of buoy 13 (Fig. 8). The shift to southerly flow was associated with a trough of low pressure, which had 1-mb amplitude, that moved northward along shore on 10 June roughly 4 h before the transition to southerly flow at each buoy (Figs. 7 and 10). This phase shift is found in most CTDs (Fig. 3; Bond et al. 1996). Figure 10 illustrates the northward propagation of this trough through a series of alongshore pressure traces from the buoys. It should be noted that the propagation discussed above is based primarily on buoy data. Strong diurnal effects at sites onshore limit the use of such data in determining propagation because southerly flow occurs at some sites as a regular part of the diurnal cycle (Fig. 7b; Beardsley et al. 1987). The time of day of this southerly flow is consistent with the decay of the strongest northerly flow just prior to the 0600 UTC climatological diurnal minimum in northerly flow at coastal sites.

The propagation is also suggested by satellite images of low clouds associated with the disturbance (Fig. 11). The movement of the cloud edge is summarized in Fig. 12. Initially, clouds were absent north of an east–west cloud edge at 0358 UTC 10 June, at about the time southerly flow began in the California Bight. Over the next 14 h, the cloud edge within ~100 km of shore surged ~320 km northward, as did the coastal pressure ridge. However, at distances >200 km offshore, the cloud edge moved southward (Fig. 12a), creating the impression of rotation in the same sense as would be

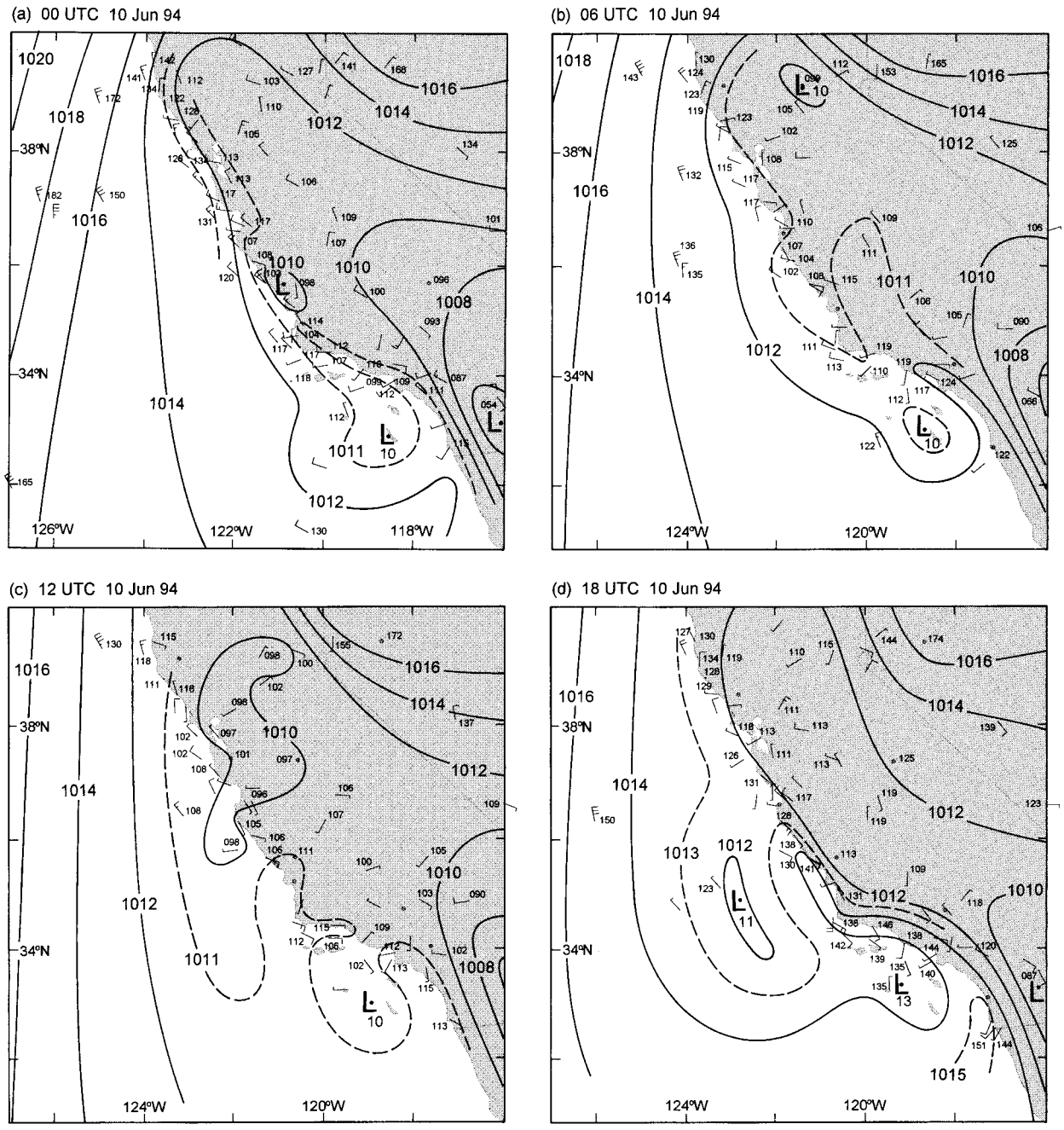

FIG. 7. Six-hourly surface observations and sea level pressure analyses (mb) between 0000 UTC 10 June and 1800 UTC 11 June 1994. MSL pressure (10*xx.x*, mb) and winds (as in Fig. 3) are plotted. An intermediate pressure contour is shown (dashed). Experimental data from several coastal sites and profiler sites are included, as are standard synoptic observations and ship reports.

expected if the coastal southerlies and offshore northerlies simply advected the preexisting cloud edge. The next phase (offshore filling) cannot be explained through advection because the cloud edge well offshore moves northward against the surface winds (c.f., Figs. 7e, 11c, 11d, and 12b). The northward alongshore progression of the cloud edge near shore between 1359 and 1810 UTC 10 June is at 8.6 m s^{-1} (or 5.5 m s^{-1} for a least squares linear fit to the four cloud-edge points in Fig. 9), which differs substantially from the 11.9 m s^{-1} propagation of the wind shift. The cloud edge continued moving northward alongshore, although more slowly, even during the pause in the propagation of the wind reversal (Fig. 9). By the time the CTD resumed its northward alongshore propagation, the cloud edge had reached the leading edge of the southerly flow. As the

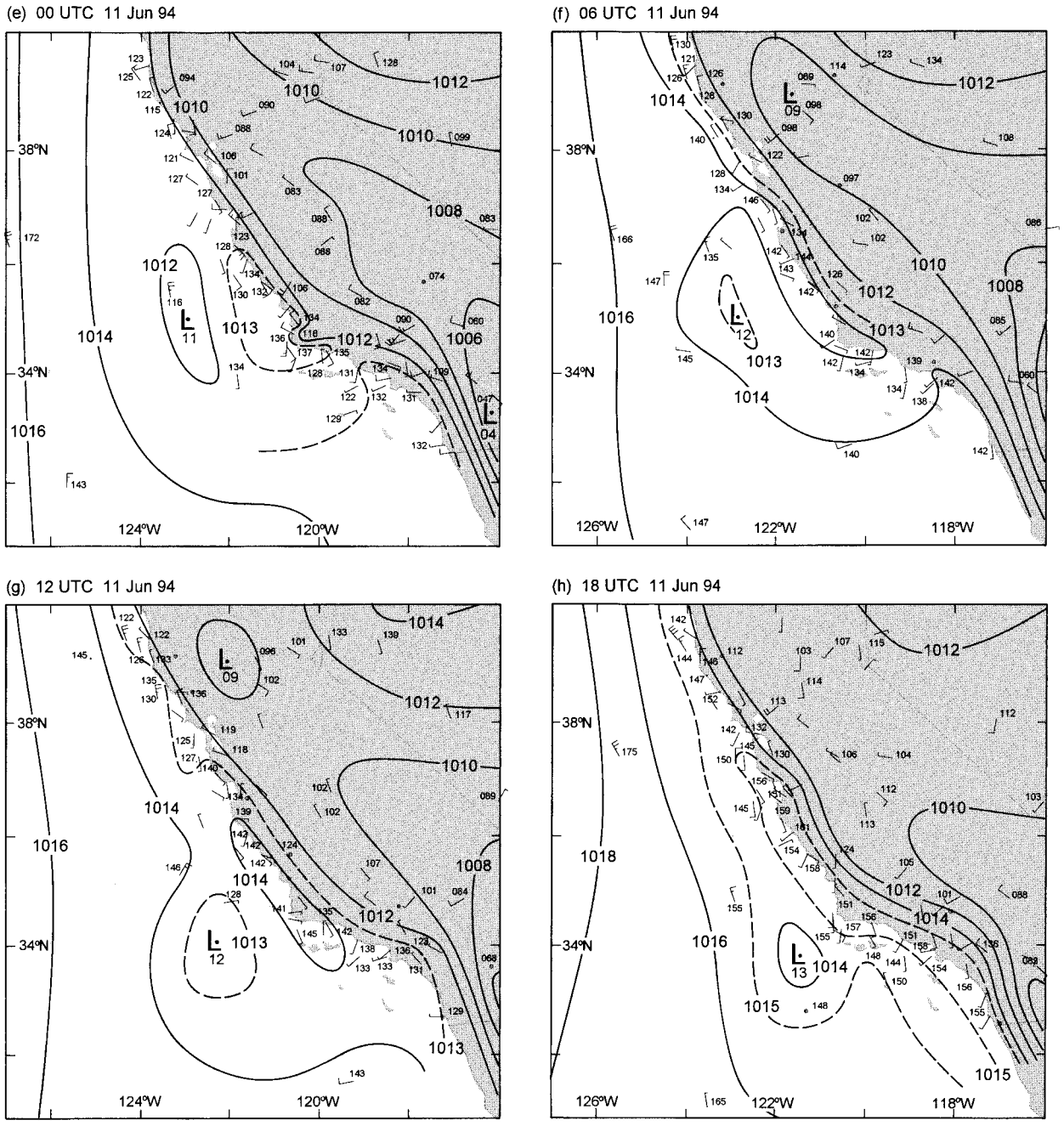

FIG. 7. (*Continued*)

northward progression of the southerly flow ended, so too did the northward development of cloud, which developed a cyclonic eddy (Fig. 12c) similar to one documented by Dorman (1985). This event indicates that the clouds cannot be used reliably to estimate the propagation of a CTD. Nonetheless, there is a correlation between the mesoscale coastal pressure ridge and the coastal cloud, as is brought out in Fig. 11 (recall that the mesoanalyses were performed independently of the satellite images).

Surface (Fig. 7e) and sounding (Fig. 13) data at 0000 UTC 11 June clearly show northwesterly flow northeast of Point Conception at a time when the flow offshore is southerly all the way to Monterey Bay, and the MBL depth was 250–300 m, which is well below the 400–500 m high crest of Point Conception. [This also occurred north of Cape Mendocino in an earlier study (see Fig. 10 of Mass and Albright 1987).] Thus, southerly flow within the MBL south of Point Conception would likely be blocked because the flow is weak ($U = 5$ m

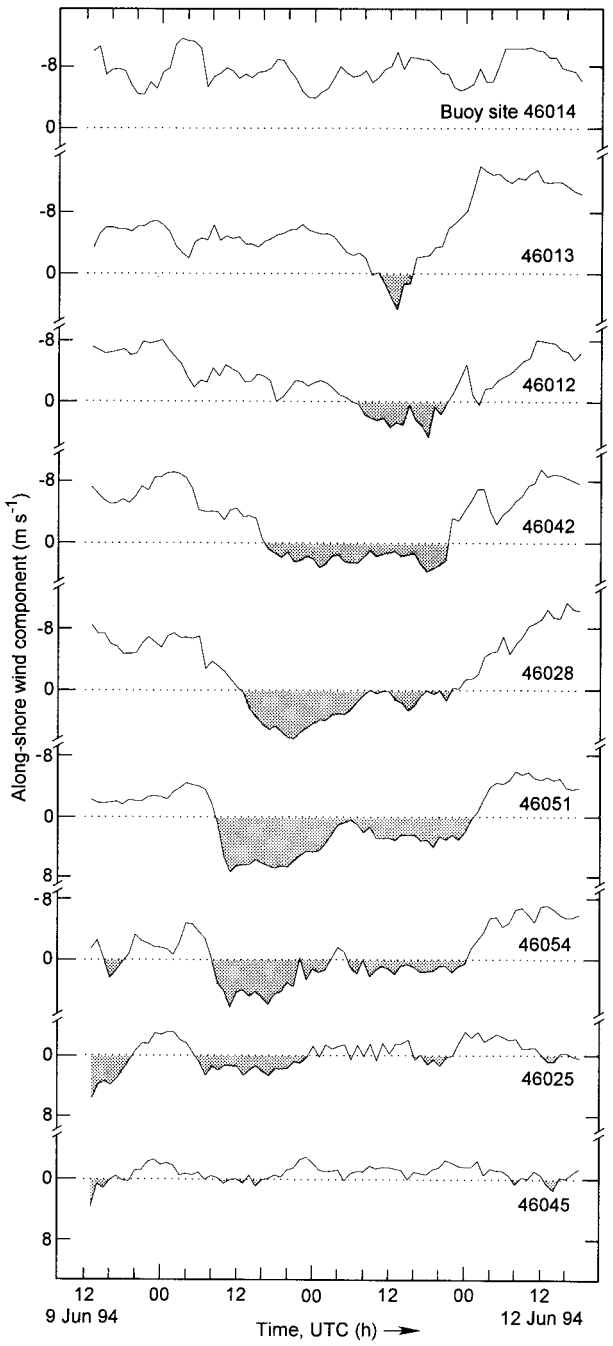

FIG. 8. Buoy-observed alongshore wind component (m s^{-1}) between 1200 UTC 9 June and 1800 UTC 12 June 1994. The shoreline orientation varies from approximately 300° to 330°, depending on the buoy location. Southerly flow is positive, but the velocity scale is inverted so that southerly flow (shaded) appears below the zero line. The northernmost buoy (near Point Arena) is at the top, the southernmost buoy (near Palos Verdes) is at the bottom. Buoy sites (labeled on the right) are shown in Fig. 1 (0000 UTC = 1700 LST).

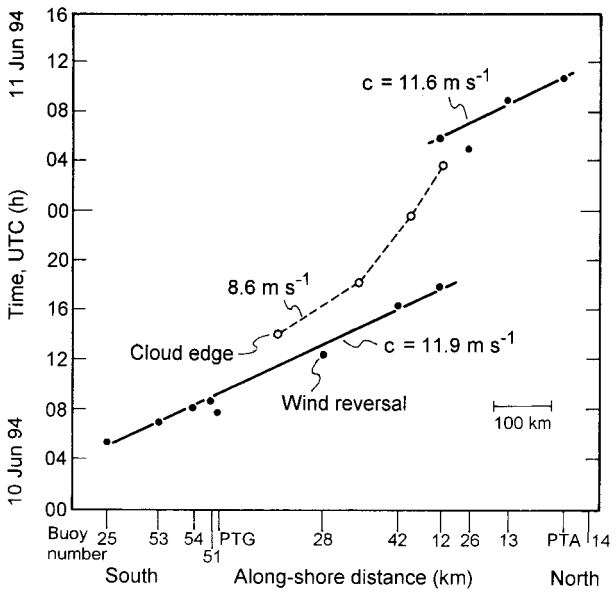

FIG. 9. Time of the observed change in sign of the alongshore wind from northerly to southerly (solid dots). The positions of the northernmost cloud edge at four times from the four satellite images shown in Fig. 11 are shown with open circles. The speed of northward alongshore progression of the wind reversal (solid lines), and of the leading cloud edge between 1359 and 1810 UTC 10 June are given.

s^{-1}) and the static stability is high ($N = 0.06$ s^{-1}), so that the Froude number (Fr = U/Nh) is ~0.2, where h is the 400-m average height of the ridge crest. Visible satellite images (Fig. 11) at 1810 and 2341 UTC 10 June show wakes around the Channel islands, and to a lesser extent also around Point Conception, that have patterns suggestive of blocking and eddy formation. The Vandenberg (VBG) sounding at 0000 UTC 11 June shows the northwesterly flow was contained within the MBL and extended only to 250–300 m at that time (Fig. 13). Because of the more frequent wind measurements made by the VBG profiler, it was possible to see that northwesterly flow never reached 650 m MSL and that the southerly flow was deflected to southwesterly for <1 h during this interval. By 1200 UTC 11 June, the eddy had disappeared, and the MBL had reached 600-m depth (Fig. 13), which was sufficient to flow over the crest of the Point Conception headland. Also, the cooling observed at VBG between 0000 and 1200 UTC 11 June below 600 m would create a 2.3-mb pressure rise under hydrostatic conditions, a value very close to the 2.4-mb rise observed by the closest buoy during the same interval, but larger than the 0.8-mb rises observed by buoys just south of the headland where the effects of the eddy would have been less.

5. Origins of the reversal in alongshore pressure gradient

A feature common to CTDs is the cessation of the northerly flow that normally dominates this region during the warm season. The northerly flow is a response to the synoptic-scale high pressure area that exists over the eastern Pacific Ocean off the United States west coast during the warm season, and to the associated

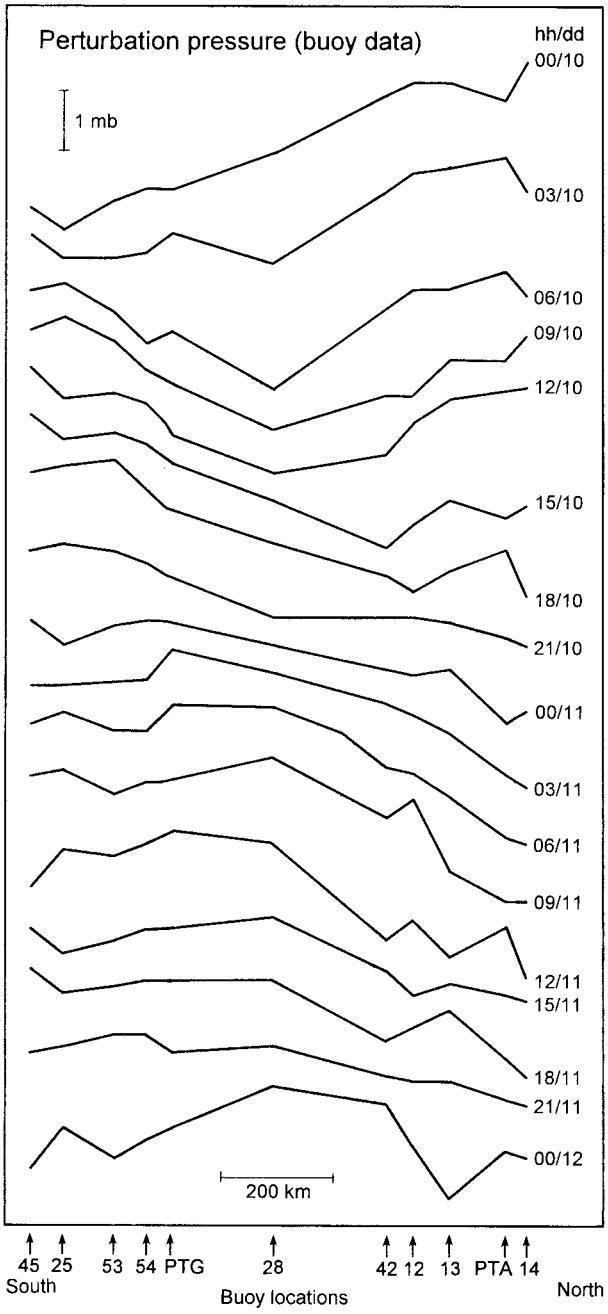

FIG. 10. Temporal sequence of alongshore pressure traces from the California Bight to near Cape Mendocino. The pressure values used are perturbations from the 72-h average at each site between 1200 UTC 9 June and 1200 UTC 12 June. Although the results are essentially the same as for absolute pressure, using the perturbation pressure allowed inclusion of data from buoy 13 and coastal station PTG that were each biased by 0.5–1.0 mb.

increase in pressure northward along the coast (Neiburger et al. 1961; Beardsley et al. 1987; Mass and Bond 1996). For a CTD to develop, it has been proposed that this northward alongshore pressure gradient must be reversed (Mass and Albright 1987; Mass 1995; Mass and Bond 1996). The evolution of the alongshore pressure gradient before and during the 10–11 June 1994 CTD is illustrated in Fig. 10, where the climatological gradient is present before 0300 UTC 10 June, followed by a period between 0300 and 1200 UTC 10 June when the relative pressure falls along the central California coast create a trough. South of the axis of this trough the alongshore pressure gradient has reversed from its climatological norm. This trough then moves northward along shore until the entire region is characterized by a reversed pressure gradient at 2100 UTC 10 June. One way this reversal of the alongshore pressure gradient can occur is to warm the atmosphere to the north more than to the south along the coast. Although there are several possible mechanisms that can cause such warming, it is likely that downslope flow off the coastal mountains and westward advection of warm continental air maximized to the north are dominant in this region during summer.

The question of whether or not such warming occurs and over what depth it occurs can be answered by combining information from the operational synoptic sounding network with special soundings launched from the Naval Postgraduate School in Monterey and frequent wind and temperature profiling by RASS and wind profilers at several sites along the coast. During the 24 h centered roughly on the initial development of southerly flow in the California Bight region, but ending several hours before the appearance of surface southerly flow near Monterey, soundings launched from Monterey revealed 3°–5°C warming below 900 mb, with substantial warming up to 800 mb and slight warming above that to 600 mb (Fig. 14). Initially, the flow was directed offshore but later became southerly above roughly 900 mb. Additional data from a wind profiler with RASS at Monterey (Fig. 15a) clearly show the gradual warming in the lowest 1.5 km from 0000 UTC 8 June through 0000 UTC 10 June. Superimposed on the typical diurnal cycle for this area is a warming of 10°–12°C over these 48 h. It should also be noted that surface temperatures on 9 and 10 June were approximately 6°C warmer than on the two previous days (Fig. 15b).

To determine the significance of the warming in relation to the observed pressure tendencies, the RASS and surface virtual temperature data were used to calculate the surface pressure hydrostatically beginning at 0000 UTC 8 June, assuming constant pressure at 1.5 km. This comparison (Fig. 15b) clearly establishes that the decreasing pressure at Monterey is due to warming in the lowest 1.5 km. Similar data are available from a 915-MHz profiler with RASS at Fort Bragg near the northernmost extent of the CTD (Fig. 16), and from Los Angeles just south of where the southerly flow developed (Fig. 17). Although the thermal data extends reliably to only 0.75 km at Fort Bragg [half the depth of the Naval Postgraduate School (NPS) and Los Angeles Airport (LAX) RASS data], the comparison between hydrostatically calculated surface pressure and the ob-

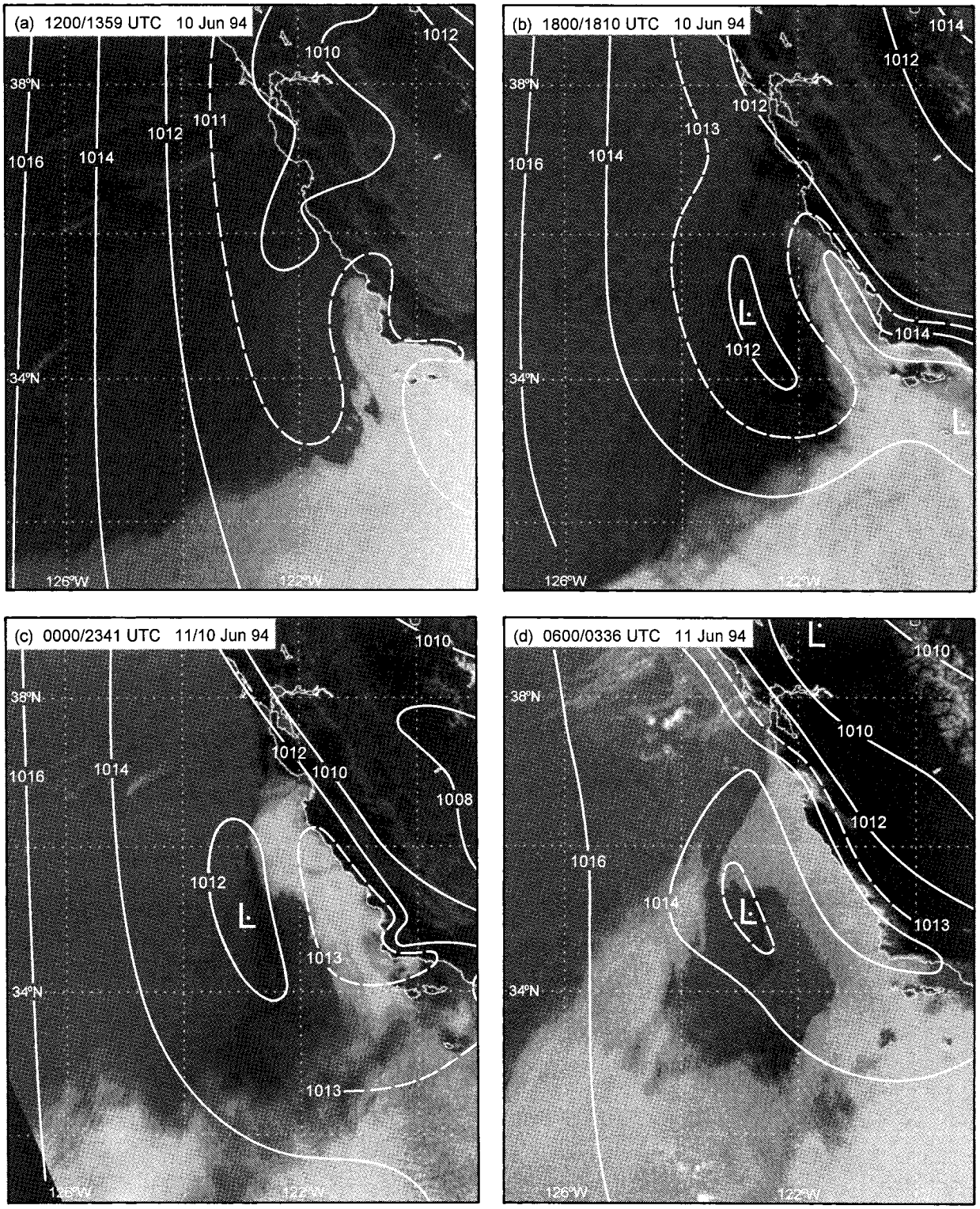

FIG. 11. Sequence of visible satellite images from a NOAA polar-orbiting satellite at 1359, 1810, and 2341 UTC 10 June 1994, and infrared image from the same satellite at 0336 UTC 11 June. Mesoscale sea level pressure (mb) analyses from the closest time in Fig. 7 are superimposed on each image. The time of each pressure analysis is shown followed by the time of each image.

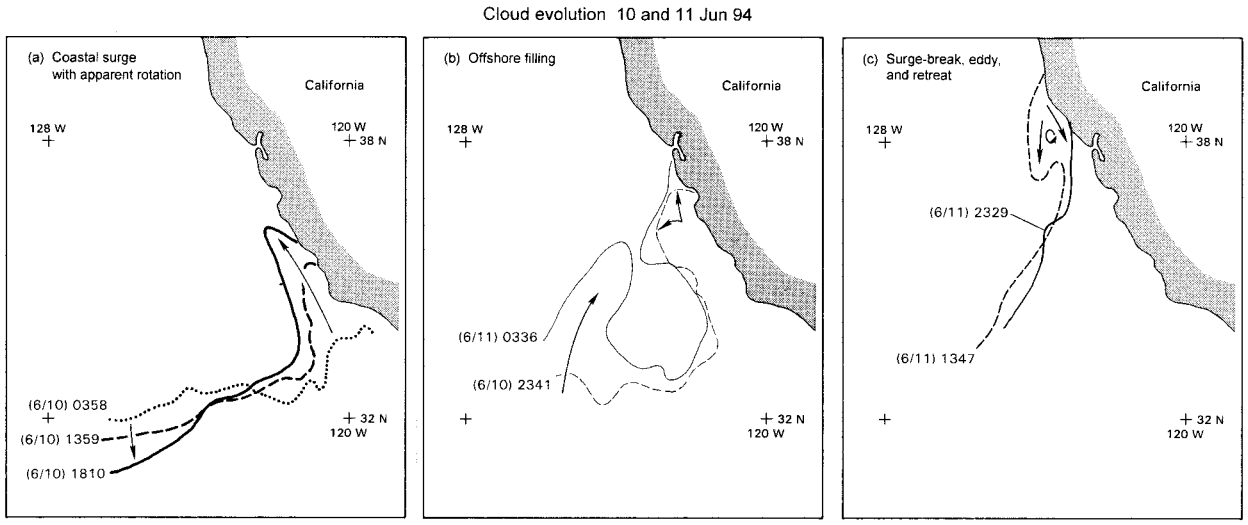

FIG. 12. Summary of the evolution of the northern edge of the extensive region of low cloud seen from visible and infrared NOAA polar-orbiter satellite images, such as in Fig. 11, representing three phases in cloud-edge development. Arrows approximate the motion of the cloud edge determined from a sequence of images. Numbers in parentheses are month/day, followed by times UTC.

served pressure indicates that the observed 10°C warming was responsible for approximately one-third of the pressure change at Fort Bragg. In contrast to the more northern sites where pressure falls were well correlated with low-level warming, the observed sea level pressure remained nearly constant during this period at Los Angeles, even though the 12°C warming in the lowest 1 km would have decreased the pressure by 5–6 mb during the same time. This indicates that cooling aloft must have compensated for the low-level warming at that site.

The warming at both Monterey and Fort Bragg occurred approximately when the flow below 1.5 km had a significant component directed offshore (Figs. 15 and 16). Recall that even though the winds at Fort Bragg were northerly during the warming, the curvature of the coastline in this area (Fig. 1) suggests that such flow is directed offshore. The Vandenberg profiler also observed easterly flow prior to the CTD near Point Conception (Fig. 5). The conclusions regarding the importance of flow directed offshore is supported by mesoscale analyses of winds and temperatures at 850 mb that suggest the strongest warm advection is along the central California coast, with weaker warm advection at that level along the northern California coast, and even

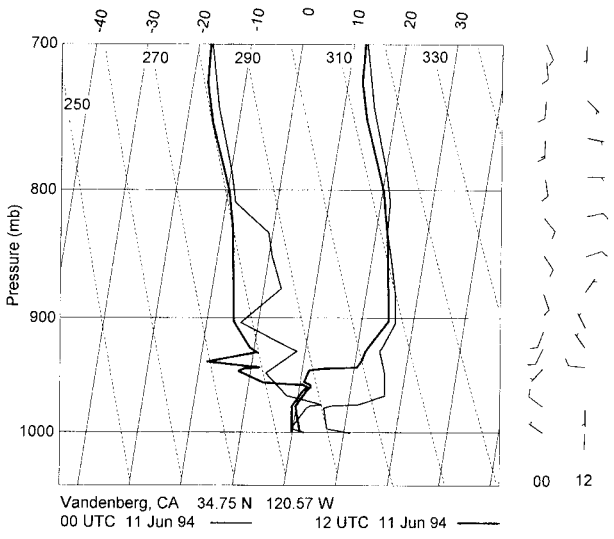

FIG. 13. Skew T–log p plot from the Vandenberg (VBG) rawinsonde ascents at 0000 (thin) and 1200 (bold) UTC 11 June. Winds are as in Fig. 3.

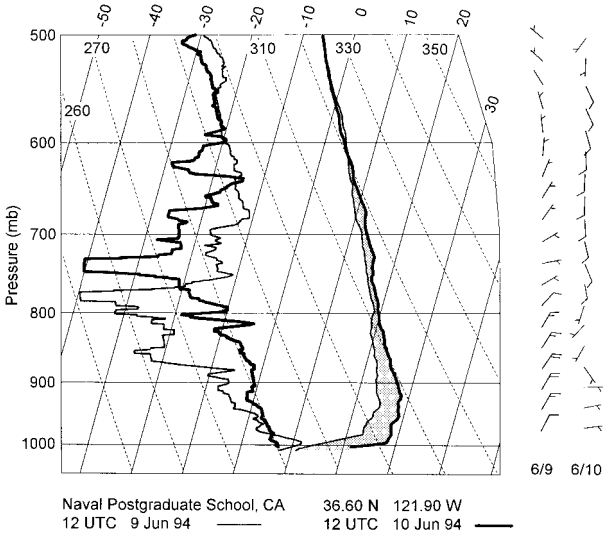

FIG. 14. Skew T–log p plot from the Naval Postgraduate School's rawinsonde ascents in Monterey at 1200 UTC 9 (thin) and 0000 UTC 10 (bold) June 1994. Shading marks warming between sounding times. Winds are as in Fig. 3.

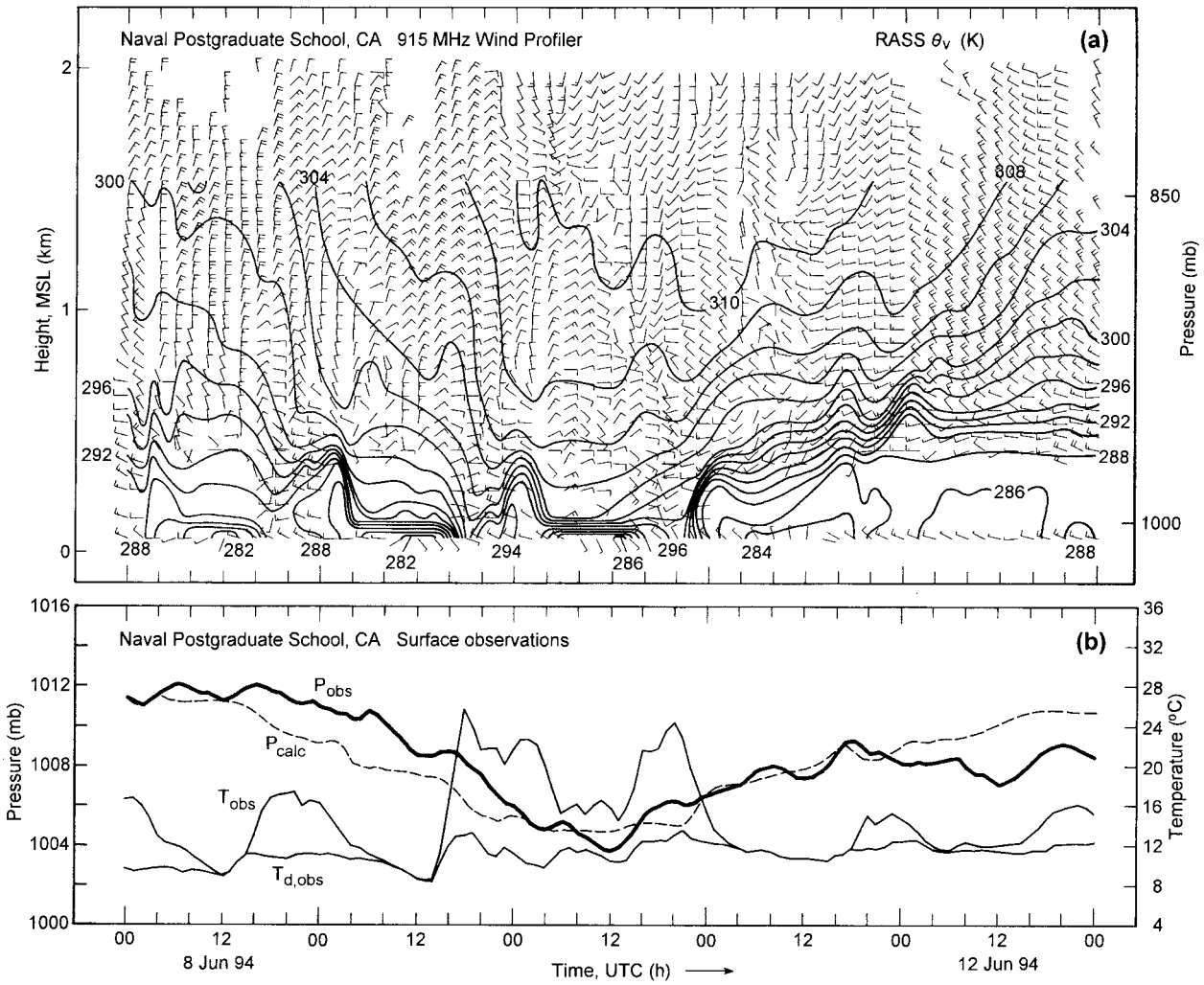

FIG. 15. (a) Time–height section of hourly RASS virtual potential temperature (θ_v, K, solid), and hourly consensus horizontal winds, from the Naval Postgraduate School (NPS) 915-MHz radar wind profiler between 0000 UTC 8 June 1994 and 0000 UTC 13 June 1994. Hourly averaged surface winds measured at the profiler site are included. Winds are as in Fig. 3. For clarity, only every other wind profile is shown. Gaps in profiler wind data are from interference due to a nearby airport surveillance radar. (b) Surface data from NPS, including observed pressure (P_{obs}), temperature (T_{obs}), dewpoint temperature ($T_{d,obs}$), and surface pressure calculated hydrostatically from RASS T_v profiles below 1.5-km altitude (P_{calc}), as described in the text (0000 UTC = 1700 LST).

cold advection north of the California–Oregon border (Fig. 3).

To better explore the relative importance of downslope warming and horizontal warm advection, calculations are made based on observed conditions and then compared with the observed warming.

Based on rawinsonde launches at 1200 UTC 9 June (a time in the middle of the 48-h period of warming) from NPS, VBG, and China Lake (NID, Fig. 1), it is possible to accurately calculate the horizontal thermal advection affecting the area centered on a point 200 km inland from the central California coast. This is fortuitous because the NID soundings were not made at many other times. From Fig. 1, it is apparent that these three stations were well situated for this calculation, which yielded a warming of 3.2 K day^{-1} at 850 mb. This compares favorably with the warming of 3–4 K observed at the three sites and the NPS RASS at that level, over 24 h around that time.

Downslope warming results from vertical air motions induced by airflow that is forced vertically by the terrain it encounters. The maximum amount of warming due to this can be estimated by the potential temperature difference between the base and top of the mountain, except in downslope windstorms, which did not occur here. The mountains near the coast rise up to 500–1500 m in California. Observations (Figs. 14–17) show that during the five days documented here the potential temperature at 1500 m was typically 10°–15°C warmer than at sea level. The timescale of the downslope-induced warming can be estimated by the time required for air to traverse from the peak to the base—that is, it depends

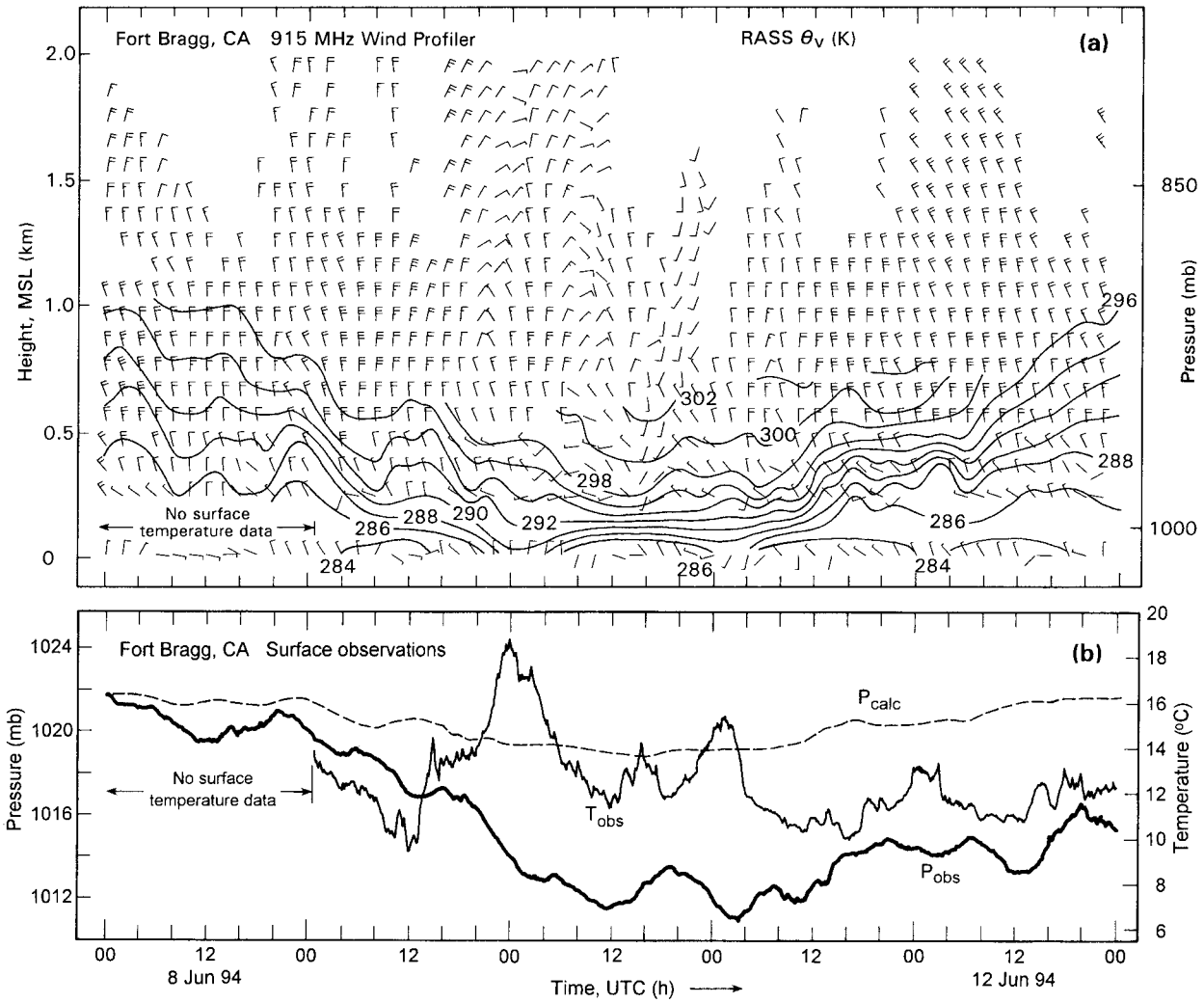

FIG. 16. As in Fig. 15 except for Fort Bragg, California. Here P_{calc} was determined from data up to 750-m altitude.

on the cross-mountain wind speed (U) and the width of the mountain. Cone peak reaches 1500 m within 6 km of the Big Sur coast, while the less steep mountains farther north near Fort Ross reach 800-m altitude about 20 km from the coast. Using the observed U and stratification, it should be expected that downslope warming would cause 7°–15°C warming. Using a range of U from 1 to 10 m s^{-1}, based on observations, this warming would be predicted to occur over 0.17–1.7 h at Cone Peak, and over 0.55–5.5 h at Fort Ross. Although the amount of warming predicted from downslope effects is close to the observed warming, it would occur more than 10 times faster than was observed.

These calculations indicate that the lower-tropospheric warming that helped precondition the central California coastal area for the development of southerly flow resulted primarily from horizontal warm advection. This warm advection is likely related to the presence of an elevated heat source (the high deserts of Nevada) and possibly downslope flow off the Sierra Nevada mountains. The changes in the synoptic-scale flow caused the westward advection of this thermal gradient representing the land–sea contrast in the lowest 1.5 km over approximately two days. Simulations of the 10–11 June 1994 CTD by Thompson et al. (1997) also indicate that warm advection played a large role, although a sensitivity to downslope warming from the immediate coastal mountain ranges was also noted. The effect of downslope warming did not appear in the observations, possibly because the wind profilers and RASS were not directly in the lee of the steepest coastal terrrain, which was around Big Sur (Fig. 1). This suggests that even greater warming and pressure falls than were observed at the profiler sites could have occurred in such places, but were not measured. However, the mesoscale sea level pressure analyses show no clear evidence of such lee troughing (Fig. 7).

An important additional consequence of the warming aloft is its affect on the MBL depth and on the strength of its capping inversion. This evolution is brought out

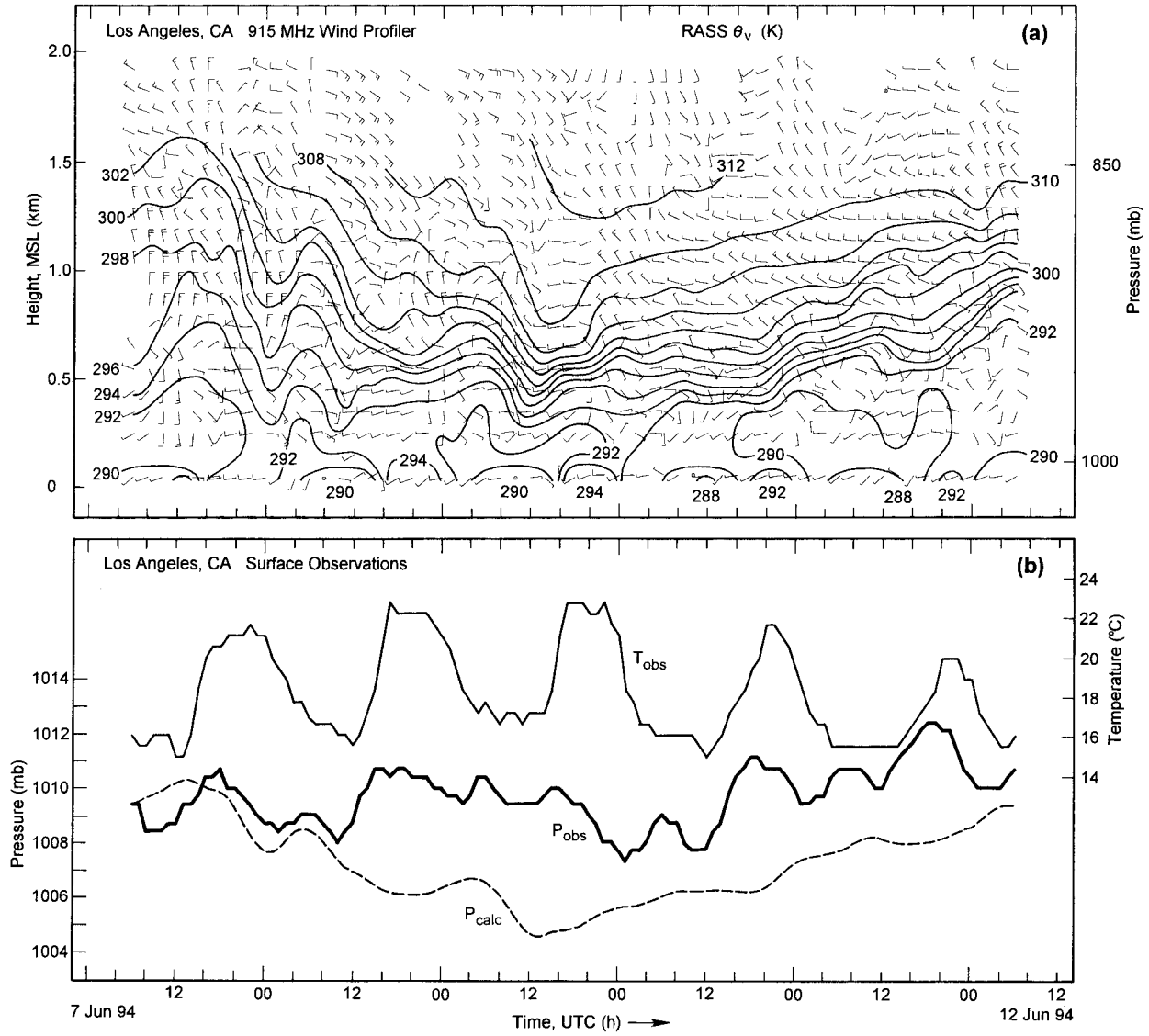

FIG. 17. As in Fig. 15 except for Los Angeles from 0600 UTC 7 June 1994 to 0600 UTC 12 June 1994.

best in the RASS data (Figs. 5 and 15–17). Monterey Bay displays a remarkably strong diurnal cycle in the MBL depth (as seen in Fig. 15a), where the MBL is hard to detect at most times, except from about 2200 to 0300 UTC each day when it is deep enough to be observed by RASS. This observation is consistent with results from an earlier sea-breeze study (Banta 1995) where balloon launches from a ship in the middle of Monterey Bay on a day with large-scale offshore flow indicated that the marine layer was absent until between 2000 and 2200 UTC when it deepened to roughly 200 m. This behavior indicates that both the 1200 UTC rawinsonde ascents from NPS (shown in Fig. 14) and a sounding from the ship *Glorita* from Monterey Bay at 1739 UTC 10 June (not shown) may not be representative of the MBL depth just outside the Bay during this event. This suggests that comparisons of the MBL depth in the Monterey area with other sites must be done with caution. If such a comparison is possible, it should be made only during the time of day when the MBL is observed there, which during the strong offshore flow characteristic of conditions before a CTD, appears to be in association with a daily deepening of the sea-breeze circulation. For the following discussion, data from 2300 to 0100 UTC are used for LAX, NPS, and Fort Bragg (FTB). (Note that the lowest height of reliable RASS data from FTB is at 258 m MSL, making it impossible to determine MBL depths below 258 m.) In the California Bight region, the MBL inversion strengthened by a factor of 4 (as measured by the lapse rate in the inversion) over 48 h ending at 0000 UTC 10 June, and by a factor of 2 at Monterey and Fort Bragg. The MBL depth (estimated as the altitude of the minimum virtual temperature in the RASS profiles) changed

by <100 m during the same time at both LAX and NPS, where it was 200–300 m. This depth compares favorably with the 280-m MBL depth observed by aircraft just north of the wind shift, as described in section 6, which helps justify the use of the 0000 UTC data from Monterey Bay.

Further evidence that the MBL was 200–300 m deep before the CTD developed is available from couplets of surface sensors deployed at several sites along the coast with one near sea level and one at higher elevation (S3/R3, S6/R6, and S7/R7 in Figs. 1 and 18). Because the temperature difference between sensors within a couplet is small when both are in the MBL, and is large when one is above the MBL, they can indicate maximum or minimum MBL depths in the vicinity of each couplet, as well as times of transitions in MBL depth. By 1200 UTC 8 June the upper site of each couplet was above the MBL, including site S7/R7 where the MBL must have been shallower than 232 m. Also, because the maximum temperatures at R7 (232 m) on 9 and 10 June were slightly higher than the maximum temperatures at R6 (470 m) on those days, it appears that the top of the MBL inversion was also below 232 m in the afternoons in that region before the CTD developed.

In contrast to the MBL, which did not change depth significantly before the CTD developed, the inversion thickness increased from 360 m to 900 m at LAX, while it stayed at 420 m at Monterey. While this data suggests that significant changes in the MBL depth did not precede the CTD, there was a large increase in the northward slope of the top of the MBL inversion just before the CTD began in the bight region.

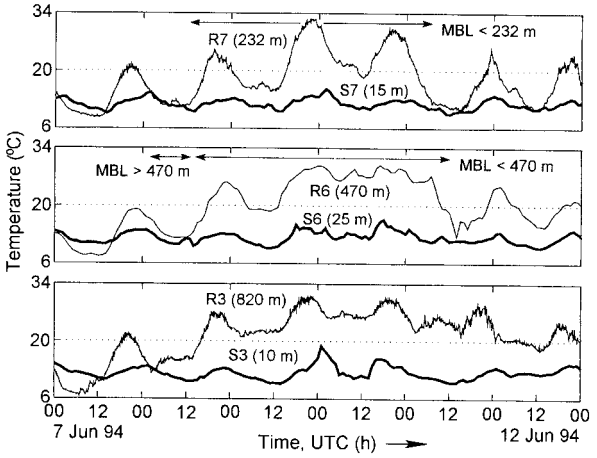

FIG. 18. Time series of air temperature (°C) observed at couplets of surface stations deployed for the experiment (see Fig. 1 for locations). Each couplet contains one site near sea level, and one on a ridge at higher elevation. Site elevations are noted in parentheses. Time intervals where the data from the couplet are adequate to conclude something about the depth of the MBL are noted.

6. Vertical and offshore structure of the region of southerly flow

a. Vertical structure at the coast

Earlier studies relied upon standard upper-level analyses and rawinsonde data every 12 h to portray the vertical structure of CTDs. These data are supplemented here with profiler and RASS data from the experiment (Figs. 5, 15, 16, 17, and 19). Southerly flow, which has traditionally been used to identify CTDs, appeared at VBG between 1200 and 1400 UTC 10 June and extended from the lowest range gate at 650 m MSL to above 5 km MSL, except for a layer of weak, easterly flow near 1.5–2.0 km MSL (Fig. 5). This is much deeper than had been pictured in any of the hypotheses concerning CTD development and propagation discussed above, and suggests that the surface low pressure center west of Point Conception (Fig. 7) may have had significant vertical extent. Aircraft data from a 0.1–2.0-km MSL vertical profile at 2000 UTC clearly shows this deep southerly flow extended at least 60 km offshore (not shown). Farther north at Monterey, southerly flow appeared above 1 km by 0000 UTC 10 June (Fig. 15a) and extended to 450 mb by 1200 UTC 10 June (Fig. 14). The profiler at Santa Cruz (Fig. 19a) showed a clear transition to flow with a southerly component, which remained below 500 m, except in a short-lived region between 1.0 and 1.5 km. As noted earlier, deep southerly flow was also present in the cases studied by Dorman (1985) and by Mass and Albright (1987).

The observed thermal structure also indicates differences from earlier conclusions that the depth of the MBL is directly correlated with the southerly flow within a CTD. This is highlighted by the time–height section of synthesized VBG profiler, RASS, and rawinsonde data (Fig. 5), which shows no change in the MBL depth at that site as the southerly flow developed. Instead, a 500–1000-m-thick layer of intermediate static stability, located between 500 and 1500 m MSL, cooled by 2°–3°C during the 12–18 h after southerly flow first appeared there. However, it should be recalled that the behavior of the MBL at VBG may have been significantly affected by an anticyclonic eddy, or expansion fan (Winant et al. 1988; Samelson 1992; Skamarock et al. 1996), created by the southerly flow around Point Conception, as described earlier. The CTD itself is marked at Monterey by cooling after 2000 UTC 10 June (Fig. 15a). Although this cooling occurs at about the same time as the cooling observed on previous days associated with the sea breeze, it is stronger, persists much longer, and extends significantly deeper. Cooling occurs not only below the stable layer near 400 m, but also in the layer above 400 m. Up to 4°–5°C cooling is found in the layer from 400 to 800 m during the 12 h after the CTD arrived. Due to the strong diurnal cycle in this region and because of the shape of the mountains around Monterey Bay, the CTD appears as westerly flow rather than southeasterly at Monterey (Fig. 15a) and at Santa Cruz (Fig. 19), and a shallow, nocturnal, southerly drainage

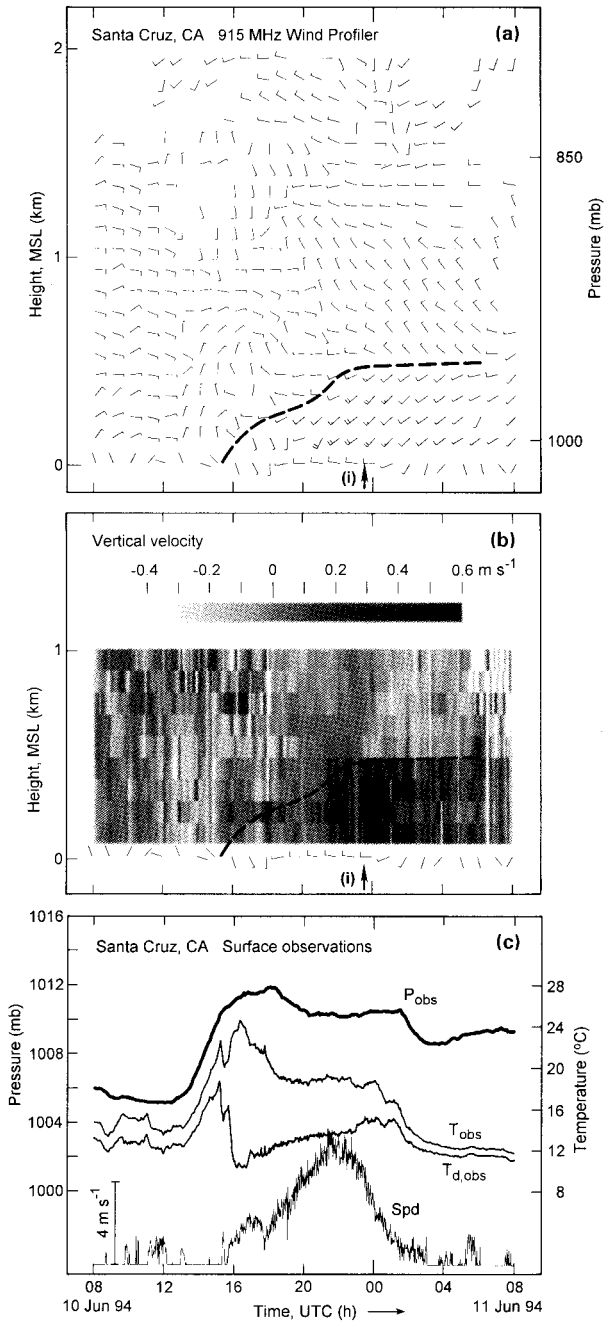

FIG. 19. (a) Hourly consensus horizontal winds from the 915-MHz radar wind profiler at Santa Cruz (SCR) between 0800 UTC 10 June 1994 and 0800 UTC 11 June 1994. Hourly averaged surface winds measured at the profiler site are included. Winds are as in Fig. 3. The dashed line roughly separates regions of southerly and northerly alongshore flow. The arrow labeled (i) marks the passage of the leading edge of low clouds. (b) Radial velocity (m s^{-1}) measured by the vertically pointing beam at SCR. Surface winds, the arrow, and the dashed line are as in (a). (c) Surface data from SCR, including observed pressure (P_{obs}), temperature (T_{obs}), dewpoint temperature ($T_{d,obs}$), and wind speed (spd) (0000 UTC = 1700 LST).

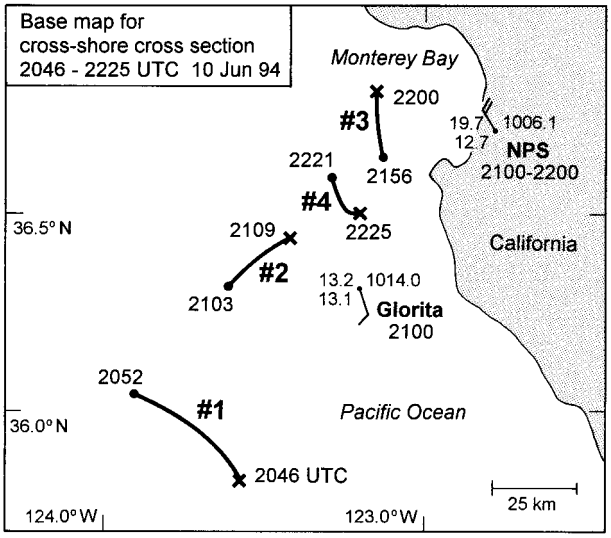

FIG. 20. Base map showing the Piper research aircraft's four flight legs (#1–#4; endpoint times UTC are shown) between 2046 and 2225 UTC 10 June 1994 that were incorporated into the cross section in Fig. 21. Surface temperature (°C), dewpoint (°C), pressure (mb), and wind velocity (as in Fig. 3) from the NPS profiler site (2100–2200 UTC 10 June 1994) and from the ship *Glorita* (2100 UTC 10 June 1994) were also incorporated into Fig. 21, and are shown.

flow down the Salinas Valley appears between 0800 and 1600 UTC on 9 and 10 June at Monterey (Fig. 15a).

b. Offshore structure

Based on the unique aircraft data from 10 to 11 June (Bane et al. 1995), it was possible to construct both alongshore and cross-shore vertical cross sections through the disturbance and its ambient environment. Data gathered during four ascents between 2046 and 2225 UTC 10 June 1994, just outside Monterey Bay (Figs. 20), are used to create a cross-shore cross section extending roughly 100 km offshore (Fig. 21). It does appear, however, that this cross section is affected by an expansion fan (Winant et al. 1988; Samelson 1992; Skamarock et al. 1996) around the Point Sur headland and into the mouth of Monterey Bay. Aircraft and wind profiler data around and offshore of Monterey Bay reveal an anticyclonic turning of the flow around the headland at the southwest corner of Monterey Bay. A 12 m s^{-1} jet of southwesterly flow was found at ~250–300 m MSL (Fig. 21a) near the entrance to the bay (in profile 9 of flight 1; Bane et al. 1995), while flow with similar direction but a bit weaker was also observed at Santa Cruz (Fig. 19). Comparison of the aircraft vertical profile and the Santa Cruz profiler data also indicate there was a downward slope toward the north side of the bay. (It should be noted, however, that conditions at the Santa Cruz site may have also been affected by its nearby terrain.) These features are consistent with the presence of an expansion fan in this area, although the sea breeze likely enhanced the southwesterly component of the

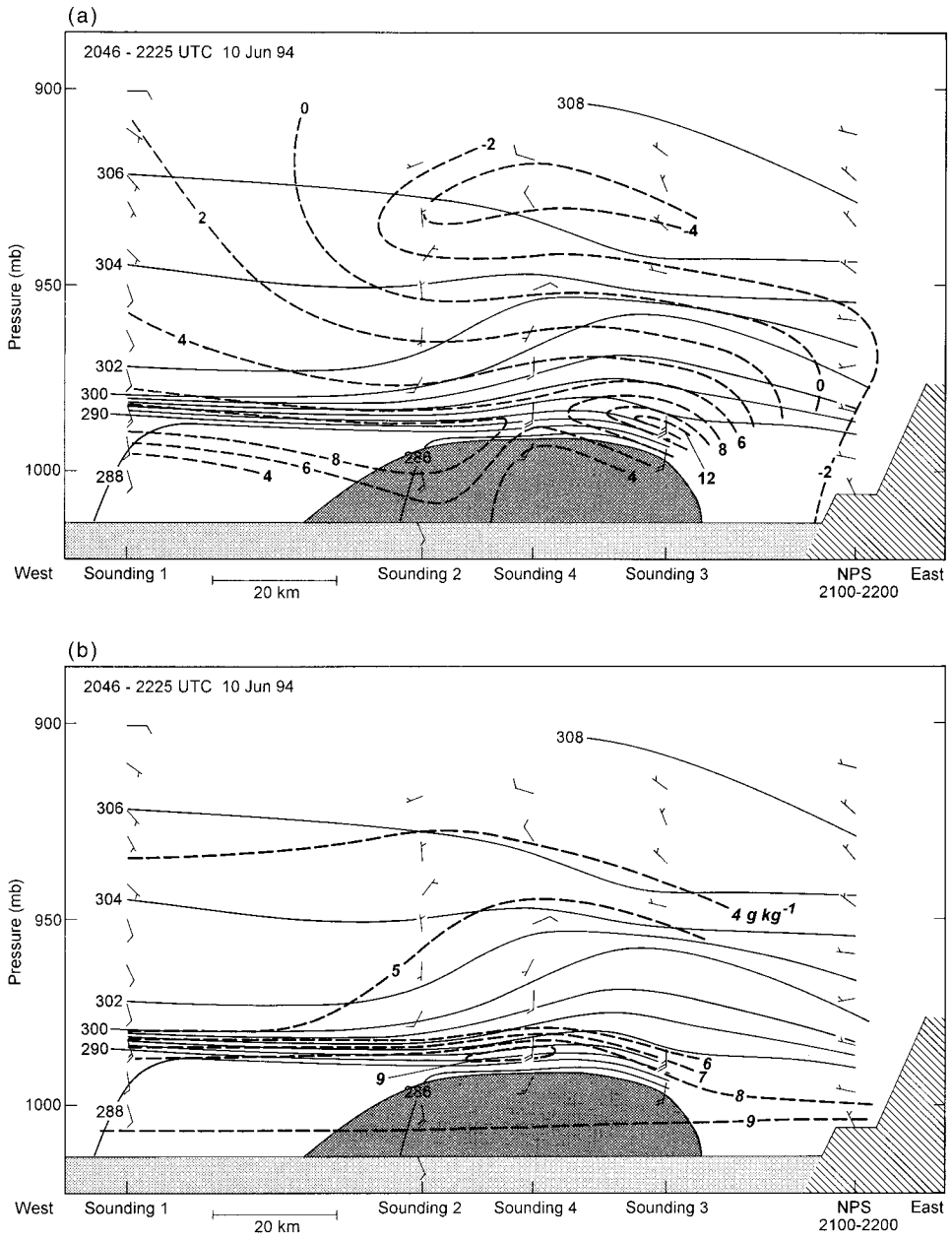

FIG. 21. Cross section of (a) potential temperature (K, solid) and alongshore wind speed (m s^{-1}, bold dashed; >0 is southerly), and (b) potential temperature (K, solid) and mixing ratio (g kg^{-1}, bold dashed), using data from the four flight legs (soundings 1–4; shown in Fig. 20) between 2046 and 2225 UTC 10 June 1994. The NPS wind profiler/RASS sounding valid between 2100 and 2200 UTC 10 June 1994 is also shown, together with offshore data from the ship *Glorita.* The dark shading marks the region of low clouds. Selected flight-level winds from the four flight legs are plotted. Winds are as in Fig. 3.

flow in this area as well. Using the aircraft vertical profile closest to the mouth of Monterey Bay (sounding 3 in Fig. 21) it is possible to calculate the internal Froude number (Fr_i). Fr_i is determined by the ratio of the wind speed (U) to the shallow water gravity wave propagation speed [i.e., $c = (g'H)^{1/2}$, where H is the depth of the MBL and $g' = g\Delta\theta/\theta_1$ is the reduced gravity based on the potential temperature difference ($\Delta\theta$) between the MBL potential temperature (θ_1) and the fluid above it]. Based on conservative choices for these parameters (H = 120 m, $\Delta\theta$ = 12 K, θ_1 = 285 K, g = 9.8 m s^{-2}, and U = 8–12 m s^{-1}), Fr_i is found to be 1.1–1.7. Thus the flow was supercritical (i.e., $Fr_i > 1$) at this point, as should be expected within an expansion fan (Freeman 1951; Winant et al. 1988; Samelson 1992).

Data gathered using a sawtooth flight pattern between

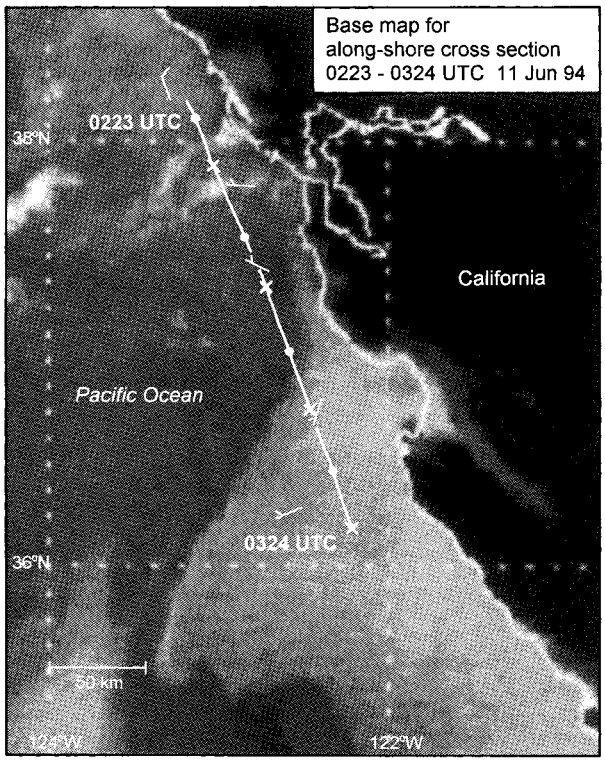

FIG. 22. Base map of the infrared satellite image at 0336 UTC 11 June 1994 showing the Piper research aircraft's flight track between 0223 and 0324 UTC 11 June 1994 that was incorporated into the cross section in Fig. 23. The dots and ×'s denote the bottoms and tops of the sawtooth flight track, respectively. Wind velocities (as in Fig. 3) from offshore buoys (42, 12, 26, and 13 from south to north) are also shown.

0223 and 0324 UTC 11 June (Fig. 22) are used to create an alongshore cross section 250 km long at a position roughly 35 km offshore (Fig. 23). This later cross section is especially useful because the northernmost profile is within the ambient environment (as indicated by the presence of northerly flow at all levels), it crosses the northern cloud edge, and it is directly over five surface observations (Fig. 22).

Contrary to expectations based on earlier studies, in which it was suggested that the MBL height would increase southward across the transition to southerly flow, the aircraft data clearly show the MBL is nearly horizontal across this transition (Fig. 23), and even becomes slightly shallower behind the transition. Similarly, the MBL depth did not decrease offshore (Fig. 21) and did not change much from earlier diurnal cycles seen in the NPS RASS data from Monterey Bay (Fig. 15). The 280-m depth of the MBL in the northernmost (ambient) of the alongshore profiles compares well with the 220-m depth at 0000 UTC 9 and 10 June, observed by RASS at Monterey well before the CTD arrived, and with the 265-m offshore depth in the cross-shore data within the perturbation. Although the MBL depth appears unaffected by the CTD passage, there is clear evidence that the 10–12 K-stable layer capping the MBL expands upward toward shore and from north to south alongshore. Although the profile closest to shore in Fig. 21 is strongly affected by the headland, the upward expansion of the stable layer was also observed farther south, roughly 50 km offshore, and well away from any headlands (not shown). This upward expansion of the MBL inversion is also manifested as an upward displacement of the 5 g kg^{-1} mixing ratio contour in both cross sections (Figs. 21 and 23).

Perhaps the most startling observation is that the southerly flow appeared first within the inversion itself (Fig. 23). This conclusion is supported both by the direct measurement of winds from the aircraft, which encountered northerly flow below the southerly flow, and by buoy observations directly beneath the flight track (Figs. 22 and 23). The southerly flow within the inversion appeared roughly 100 km north of the position of the wind transition at the surface. Because the surface wind transition is the basis for measuring the propagation of the CTD, it appears likely that the southerly flow within the inversion also propagated northward alongshore. However, because observations of this phase relationship are not available at other times, it remains uncertain that the wind transitions at the surface and in the inversion have the same relationship during the propagating phase. Although this uncertainty remains, numerical simulations of this CTD presented in Thompson et al. (1997) also indicate that southerly flow first appeared above the surface, within the MBL inversion.

The clouds were less than 200 m deep, and appeared in an interesting region in the alongshore cross section (Fig. 23). Although the MBL depth did not change substantially from north to south across the leading edge of the CTD, there was a slight ($<$100 m), local decrease in its depth near the middle of the cross section. The cloud appeared south of this region, where the MBL had returned to its original depth (Fig. 23). It is also interesting to note the southward increase in mixing ratio both at the surface and in the lower aircraft measurements (Fig. 23b). This may suggest that northward alongshore advection of slightly warmer and more moist air within the southerly flow over the generally cooler waters to the north may contribute to the formation of fog that often accompanies CTDs. This inference is also supported by the presence of fog, because it can be formed by heat conduction to the surface. In contrast, vertical air motions measured directly by the wind profiler at Santa Cruz (Fig. 19b) provide evidence that lifting was involved in cloud formation. Although the vertical motion was initially downward at 20–30 cm s^{-1} from 0800 to 1600 UTC, it became upward at 30–40 cm s^{-1} within the region of southerly flow below 0.5 km from 2130 UTC 10 June to 0130 UTC 11 June, which is centered on the time that clouds and fog appeared at the site—that is, 2330 UTC 10 June.

These observations indicate that this CTD is best

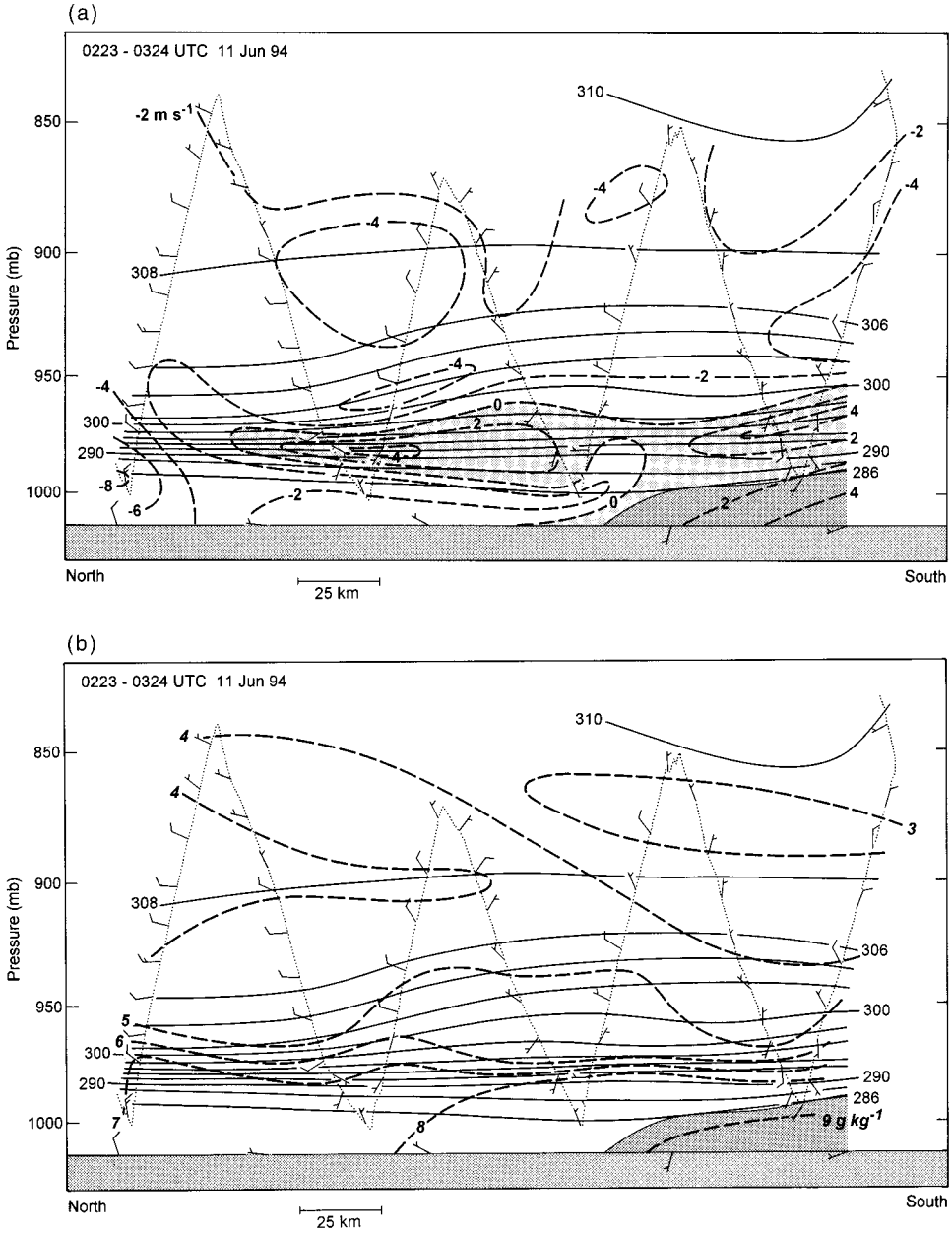

FIG. 23. Cross section of (a) potential temperature (K, solid) and alongshore wind speed (m s^{-1}, bold dashed; >0 is southerly and shaded lightly), and (b) potential temperature (K, solid) and mixing ratio (g kg^{-1}, bold dashed), using data between 0223 and 0324 UTC 11 June 1994 from the flight track shown in Fig. 22. Data from offshore buoys are also shown. The dark shading marks the region of low clouds. The flight track is depicted with a small dotted line, with selected flight-level winds shown. Winds are as in Fig. 3.

characterized using a three-layer system where the MBL inversion expands upward and pushes slightly downward on the MBL as the southerly flow appears first within the inversion. This behavior brings into question the applicability of the traditional shallow water model (e.g., Gill 1982; Dorman 1985; Reason and Steyn 1992) to this phenomenon. This is highlighted by the fact that the most perturbed layer in the observations is the same layer that the two-layer idealization assumes is infinitely thin.

c. Evidence of a delayed deepening of the MBL

Although the southerly flow developed without the expected increase in MBL depth from its original 200–300-m depth, there is evidence that the MBL did deepen

later, before the southerly surface flow ceased. This is seen at VBG by comparing soundings at 0000 and 1200 UTC on 11 June (Fig. 13), which indicates that the MBL deepened there 15–27 h after southerly flow developed offshore of that site, and 14–26 h before the southerly flow ended there. At LAX, the RASS data (Fig. 17) reveal an increase in MBL depth beginning at 2000 UTC 10 June, 15 h after the southerly flow first developed in the California Bight and 4–26 h before the southerly flow ended there (Fig. 8). At NPS, the RASS data show that the MBL deepened from the depth it had during the sea breeze on earlier days beginning at roughly 0600 UTC 11 June (Fig. 15), 14 h after the CTD arrived there, and 16 h before the southerly surface flow ended there. During this phase the MBL roughly doubled in depth over 12–14 h at each site. It deepened by 200–300 m at LAX, by 300–400 m at VBG, and by 200–300 m at NPS. By the time the aircraft flew at 2100 UTC on 11 June (not shown), the MBL offshore had deepened by 190 m from 210 m to 400 m in the same region as shown in Figs. 22 and 23.

Farther north, near the northernmost extent of the surface southerly flow, a different sequence of events was observed on 11 and 12 June. Based on the surface data at S6/R6 and S7/R7 (Fig. 18), and on the buoy data offshore (Fig. 8), the MBL deepened in that region between 0500 and 0700 UTC on 11 June, 3–5 h before the brief period of southerly surface flow in that area. In addition, FTB reported an increase in MBL depth beginning at roughly 1100 UTC 11 June, even though surface southerly flow associated with the CTD never reached that far north.

Along the central California coast, where the CTD was well defined, the MBL deepened by roughly 200–300 m, beginning 12–14 h after the surface wind shift. This deepening of the MBL progressed northward along shore with time, and propagated beyond the northernmost extent of the surface southerly flow.

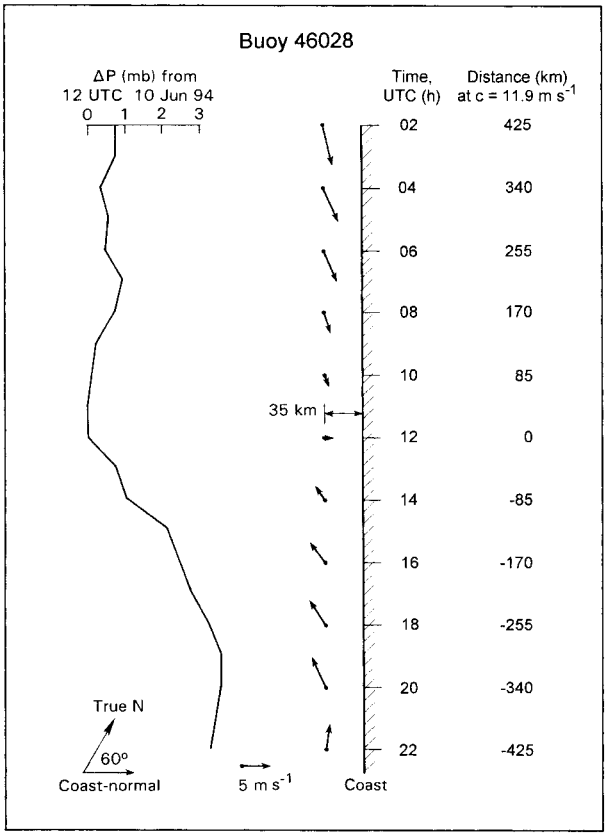

FIG. 24. Surface data from buoy 28, which is 35 km offshore, showing the time series of pressure (mb) and wind (scale shown) relative to the coastline. The vertical axis is time starting at 1200 UTC 10 June, and distance based on an 11.9 m s^{-1} phase speed.

7. Implications concerning the origin and nature of the southerly flow

The observations in this event can be used to test the various hypotheses put forth to describe the dynamical behavior of CTDs. This section describes the implications of the observations with regard to these concepts, although more thorough treatment of this issue is left for future study. The emphasis here is on the behavior of the leading transition, which is clearly associated with the surface wind shift, rather than on the delayed deepening of the MBL, which is less well observed. It is also important to note that synoptic-scale changes (Reason and Steyn 1995) and diurnal effects complicate the interpretations of the CTD observations.

a. The gravity current hypothesis

The gravity current concept, which appeared to apply best to the latter stage of a case studied by Mass and Albright (1987) and was proposed to explain several other events (Dorman 1987; Beardsley et al. 1987; Hermann et al. 1990), appears to be untenable in this event. The advective character of a gravity current requires that some portion of the denser fluid must move at least as fast as the leading edge of the dense air (Simpson 1987). Because the maximum observed southerly flow was <8 m s^{-1}, and the disturbance propagated northward along shore at 11.9 m s^{-1}, this important aspect of gravity current behavior is violated. In addition, the observed changes in wind, temperature, and pressure are too slow to be considered as resulting from a gravity current. This is illustrated first by a representative time series of wind and pressure at buoy 28 (Fig. 24), where the complete wind transition occurred gradually over several hours, starting as a weakening of the northerly flow. The pressure at that site did increase after the southerly flow appeared, but 1–2 mb of that is likely the result of semidiurnal atmospheric tides. However, the 1-h sampling of the buoys could mask more abrupt transitions. This is addressed using data from one of the special coastal observing sites that made measurements every minute (Fig. 25). At this site just south of Monterey Bay, the transition to persistent southerly flow

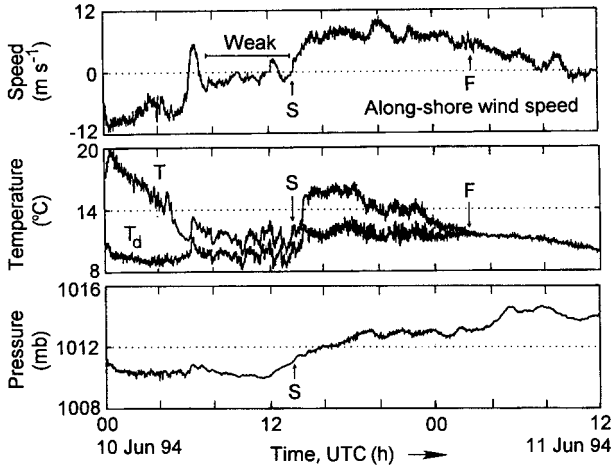

FIG. 25. Surface observations of alongshore wind (m s^{-1}), temperature (°C), dewpoint temperature (°C), and surface pressure (mb) from a site just south of Monterey Bay (S3 in Fig. 1). S marks the start of the southerly flow associated with the CTD, and F marks the appearance of fog. ''Weak'' denotes a period of weak flow.

(preceded by two brief periods of southerly flow) occurred near 1400 UTC with a 3 m s^{-1} wind shift over a few minutes followed by an acceleration of 5 m s^{-1} over 1 h. The pressure rose at this time by <0.5 mb. Although such transitions can mark weak gravity currents, the 3°C temperature increase associated with the event is opposite in sign from the cooling that would be consistent with gravity current behavior.

b. The Kelvin wave hypothesis

Another hypothesis is that a Kelvin wave is created when the MBL is forced upward along a portion of the coast, and Coriolis effects trap the disturbance along the coastal mountains (e.g., Gill 1977; Maxworthy 1983; Dorman 1985; Reason and Steyn 1992; Samelson and Rogerson 1996). The alongshore variation of pressure and wind is consistent with what is expected for a linear Kelvin wave (e.g., Gill 1982), in that northerly flow is found in the region of minimum pressure to the north, while the strongest southerly flow is found under the mesoscale coastal ridge (Fig. 7). As pointed out by Gill (1982, 378) this phase relationship occurs because the alongshore winds in a Kelvin wave are in geostrophic balance with the cross-shore gradient of the layer's depth in the shallow water system. The phase relationship is brought out further through time–space analysis of the alongshore and cross-shore components of the surface winds at buoy 28 (Fig. 24), which is located along a very straight stretch of coastal mountains (Fig. 1). From this, it is evident that the northerly flow gradually weakened over several hours, and the southerly flow increased over a similar timescale. This result is also evident at other buoys shown in Fig. 8. The switch to southerly surface flow occurred near the time that pressure began increasing, and its intensity increased as the pressure rose ~3 mb (although 1–2 mb of this could be attributable to diurnal and semidiurnal effects). It has also been shown (Samelson and Rogerson 1996) that a linear Kelvin wave model forced by climatological conditions that Mass and Bond (1996) found associated with most CTDs reproduces several features consistent with mean CTD behavior. This conclusion also applies to the event studied here: a pressure minimum passes a site before the transition to southerly flow, transitions occur over several hours at a given site, southerly flow is associated with a mesoscale coastal ridge, the disturbance decays offshore, enhanced northerly flow occurred to the north, easterly flow preceded the CTD development, and a coastal low was present offshore.

However, the Kelvin wave concept has traditionally involved changes in the MBL depth resembling a full cycle of a wave, whereas the observations show a change in the inversion thickness and little change in the MBL depth. It may be possible to still consider the perturbation as a Kelvin wave, but with a higher-order vertical structure. Nonetheless, the semipermanent thickening of the MBL inversion still differs from the traditional view that a solitary Kelvin wave includes a limited region of elevated MBL along shore. Because of the semipermanent character of the observed perturbation, in this respect the event resembles an internal atmospheric bore (e.g., Klemp et al. 1997). However, the smoothly sloping, leading edge of the disturbance (Fig. 23), differs from the steep leading edge of a traditional bore. The turbulence created at this steep leading edge is an important factor in bore dynamics, and it has now been shown (Klemp et al. 1997) that most of the energy is lost into the upper layer in atmospheric bores, rather than into the lower layer. Although simulations (Klemp et al. 1997) indicate that this energy loss occurs through turbulence, it is possible that upward gravity wave radiation could act in a similar capacity (W. Skamarock 1996, personal communication). This opens up the possibility that gravity wave radiation could be effective enough to prevent or delay the collapse of the leading edge of an atmospheric internal bore into a steep discontinuity. However, because the turbulence occurred behind the leading edge, the initial upward perturbation of the interface in the simulated bores can be smooth, but is still 100 times steeper than the observed slope of 3×10^{-3}.

c. Ageostrophic downgradient response to an alongshore pressure gradient: The isallobaric wind

Another hypothesis argues that the southerly flow is an ageostrophic mesoscale response to a reversal of the alongshore pressure gradient, where the northward alongshore decrease in pressure drives the acceleration of the southerly flow (Mass and Albright 1987). The reversal of the pressure gradient could be a response to the extension of troughing to the coast (Mass and Albright 1987; Mass and Bond 1996), or to the blocking

of geostrophic westerlies by the mountains (Dorman 1985; Rogerson and Samelson 1995; Samelson and Rogerson 1996).

The total ageostrophic flow is defined by Eq. (1) (e.g., Bluestein 1986):

$$\mathbf{V}_a = \frac{1}{f}\mathbf{k} \times \frac{D\mathbf{V}}{Dt}, \tag{1}$$

where $\mathbf{V}$ is the total wind velocity, $\mathbf{V}_a$ is the ageostrophic wind velocity, f is the Coriolis parameter, t is time, and $\mathbf{k}$ is the vertical coordinate vector. The total ageostrophic wind includes the effects of local time tendencies of the geostrophic and ageostrophic wind, the vertical and horizontal advection of momentum, surface friction, and viscosity (e.g., see Bluestein 1986). All of these terms can contribute to the component of the ageostrophic flow that it is directed down the horizontal pressure gradient. However, the most direct link to the concept of an ageostrophic downgradient response to a reversal (i.e., a temporal change) in the alongshore pressure gradient that was explored by Mass and Albright (1987) is in the term referred to as the isallobaric wind. The isallobaric wind represents the local time-rate-of-change of the geostrophic wind [Eq. (2)]:

$$\mathbf{V}_i = \frac{1}{f}\mathbf{k} \times \frac{\partial \mathbf{V}_g}{\partial t}, \tag{2}$$

where $\mathbf{V}_i$ is the isallobaric wind velocity and $\mathbf{V}_g$ is the geostrophic wind velocity. Substituting the geostrophic wind relationship into Eq. (2) yields the Cartesian components of the isallobaric wind. The north–south component is given by Eq. (3),

$$v_i = -\frac{1}{f^2\rho}\frac{\partial^2 P}{\partial y \partial t}, \tag{3}$$

where v_i is the north–south component of the isallobaric wind, ρ is density, P is pressure, y is horizontal distance (positive directed northward; alongshore in this study). It is apparent that v_i results from the time-rate-of-change of the alongshore horizontal pressure gradient, or the north–south gradient of the time-rate-of-change of sea level pressure. Such gradients are capable of inducing flow from a region of relative pressure rises toward a region of relative pressure falls (Brunt and Douglas 1928; Gill 1982).

As shown in Fig. 3, there existed significant alongshore gradients of the local pressure tendency. The isallobaric wind can be calculated from Eq. (3) using the observed pressure tendencies at buoys 51, 53, 54, and 28 over 6-h intervals on 10 June 1994. For 0000–0600 UTC between buoys 28 (−1.8 mb) and 51 (−0.6 mb), which are 183 km apart, the isallobaric wind is southerly at 3.5 m s^{-1}. Similarly, the pressure change (−0.05 mb) at buoys 53 and 54 (which is averaged here because they are near the Point Conception headland) can be compared with buoy 28, which is 240 km away, and yields a southerly isallobaric wind of 3.9 m s^{-1}. The same sets of stations both yield 0.3 m s^{-1} isallobaric wind based on pressure changes between 0600 and 1200 UTC 10 June. The period from 1200 to 1800 UTC yields isallobaric winds of −0.6 and −0.1 m s^{-1} for buoy sets 28–51 and 28–53/54. Similar pressure tendency gradients are evident farther north later in the period (Fig. 3), suggesting that the region influenced by this mechanism propagated northward alongshore, as did the CTD.

These results indicate that the isallobaric wind was southerly and was strong enough to be a significant fraction of the observed weakening of the northerly flow between 0000 and 1200 UTC 10 June in the vicinity of the buoys used in the calculation. Although the isallobaric wind calculated here was too weak to reverse the northerly flow itself, it appears to play a role in creating the transition. It remains unclear, however, what the contribution to the total downgradient ageostrophic flow is from the advective, frictional, and other terms that are not considered here.

d. The possible role of potential vorticity generation by friction along coastal mountains

It has been proposed that PV anomalies can be generated by the interaction of flow with steep terrain (Thorpe et al. 1993; Schär and Smith 1993), and that conditions along the northern California coast may have been conducive to PV generation in this case (Persson et al. 1995; 1996). This mechanism requires that a layer of strong stratification and strong alongshore winds (i.e., the MBL inversion) intersect the coastal mountains in a way that causes a strong horizontal gradient of friction. The PV generated in this way would be focused in the MBL inversion and could then be advected by the background flow. In the current study, the PV generation would have occurred north of the CTD along the coastal mountains of northern California, and a PV plume would have been advected south-southwestward. Persson et al. (1995, 1996) showed that the plume of PV produced by a numerical simulation of the 10–11 June 1994 event was of a shape and strength that could induce (Joly and Thorpe 1990) a cyclonic circulation consistent with the horizontal shear of the alongshore flow documented offshore by SSMI satellite-observed surface winds (Fig. 6). It could also have produced westerly flow at its southern end within the bight region, thus possibly playing a role in initiating the CTD as well as preconditioning the coastal environment by reducing or removing opposing northerly flow along the central California coast.

8. Summary and conclusions

The CTD of 10–11 June 1994 had characteristics common to most CTDs observed earlier in the area using buoys (Bond et al. 1996) and occurred in a synoptic environment similar to those found to be typical for such

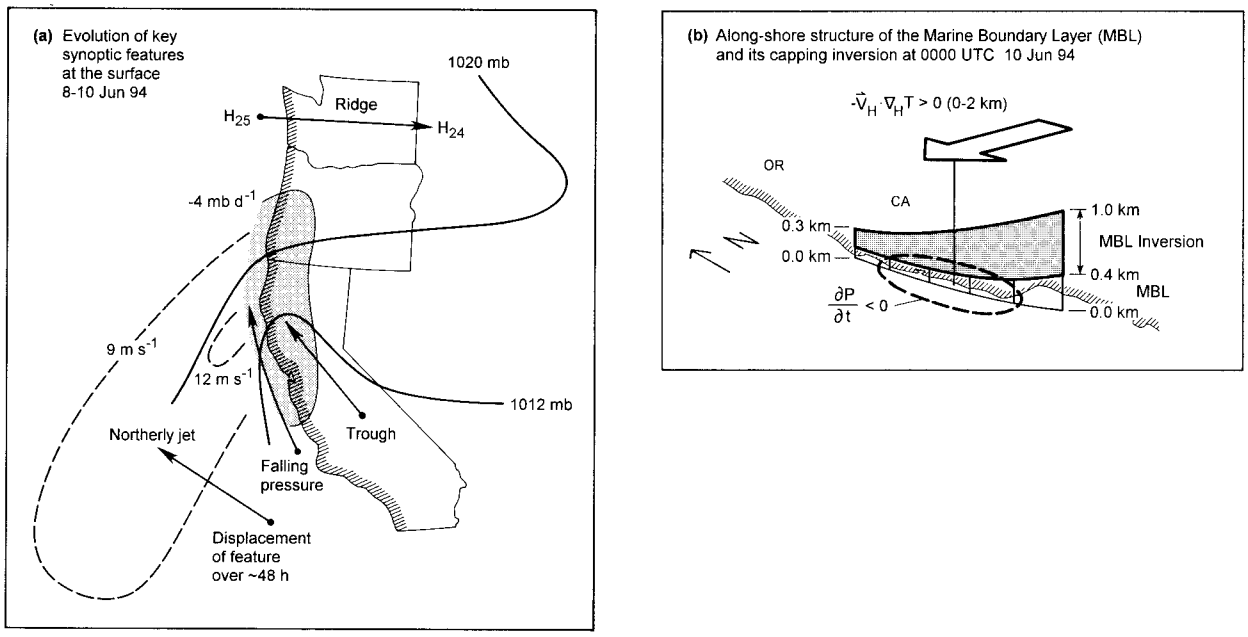

FIG. 26. (a) Synoptic overview of preconditioning before southerly alongshore flow developed. Arrows and dashed lines represent the movement over approximately 48 h of the feature at the end of the arrow. (b) Vertical structure of MBL inversion, and the relationship between the region of coastal pressure falls and lower-tropospheric warm advection.

events (Mass and Bond 1996). It moved northward alongshore at 11.9 m s^{-1}, contained southerly flow attaining 7 m s^{-1}, and extended over 700 km of coastline. The evolution of the synoptic environment in this case is summarized in Fig. 26. Key features (Fig. 26a) include the onshore movement of a surface high pressure ridge into the Pacific Northwest, the northward development of the thermal trough into northern California, the displacement of the northerly or northwesterly alongshore jet westward away from the central California coast, and pressure falls of 2–6 mb over 24 h along 600–1000 km of the coast. The pressure falls result primarily from 10° to 12°C warming over 48 h in the lowest 2 km MSL (Fig. 26b). Data in central California establish that the warming in that area is a consequence of westward advection of warm, continental air, although some downslope warming may have been locally important in regions of tall, coastal mountains, as has also been found in recent, real-data simulations of this event (Thompson et al. 1997). This caused the climatological alongshore pressure gradient to reverse along the central California coast where the CTD developed, and also modified the cross-shore pressure gradient in a way that weakened the geostrophic northerlies at the coast. By the time the CTD began, this large-scale environment caused the MBL and its capping inversion to slope downward to the north, with the MBL and the top of its capping inversion dropping to below 300 m (Fig. 26b). The slope of the inversion top was much greater than the climatological slope in the region during June (Neiburger et al. 1961).

The CTD of 10–11 June 1994 along the California coast propagated northward along shore, as evidenced by several features, including the alongshore wind component, an alongshore pressure trough, and clouds. Although the clouds did move north, they were not in phase with the transition to southerly flow. The northward development of the cloud edge differed from nearby wind measurements, and it progressed northward alongshore more slowly than did the transition to southerly surface winds. One of the wind profilers directly measured 30–40 cm s^{-1} lifting when cloud appeared at that site. However, the exact relationship between the kinematic behavior and clouds in this CTD remains unclear, but has been explored in Dorman et al. (1998).

Once the southerly flow developed around Point Conception, it propagated northward alongshore with gradual transitions in wind, pressure, and temperature at the surface. In contrast to earlier studies, deep (>2 km) southerly flow, and 2°–4°C cooling between 500 and 1500 m was observed in association with southerly flow at the surface and the northward extent of the southerly flow was greatest within the MBL inversion. The gradual transitions observed in wind and pressure, along with the temperature increase at the time of transition to southerly flow, indicate that the observed behavior is not well characterized as a gravity current. However, Dorman et al. (1998) suggest that some small-scale features seen in surface data represent a weak gravity current. Although final conclusions regarding the best dynamical interpretation of this event are left to other work, limited analyses presented here suggest that some characteristics were consistent with Kelvin wave or internal bore behavior, and that ageostrophic northward

accelerations due to the alongshore pressure gradient contributed significantly to the development of southerly flow through the isallobaric wind.

Rather than the deeper, nearshore MBL associated with CTDs, as proposed by most earlier studies, the aircraft, profilers, and RASS documented that the MBL remained nearly horizontal in the region where southerly flow first developed, except around headlands where it lowered as part of the expansion fan/hydraulic jump phenomena. However, the inversion capping the MBL well offshore was found to expand upward toward shore and toward the south, creating a 300–500-m-deep layer of strong static stability between the cool MBL and the warm free troposphere. The observations also clearly showed that the southerly flow extended farther northward alongshore within the inversion than at the surface, indicating that at a specific site the southerly flow would appear first within the inversion, and then at the surface as the CTD propagated by. Evidence was also presented that the MBL did deepen by 200–300 m later in the event and that this feature also propagated north, trailing the shift to southerly flow at the surface by 12–14 h along the central California coast. The origins of this deepening of the MBL and its northward propagation remain unclear.

These findings suggest that future idealized models of CTDs may need to retain much more vertical structure in the stratification, and likely will require at least three layers rather than two. The complexity of this event, which appears to be an event representative of many other less well-documented cases, may indicate that CTDs can be influenced by several dynamical mechanisms that modulate their propagation and structure. Further work is required to establish which mechanisms are important in most cases, how the clouds form, what triggers a CTD, and whether CTDs can be reliably predicted by mesoscale forecast models.

Acknowledgments. Both the experimental and analysis work on which this paper is based were partially supported by grants from the Office of Naval Research as part of the Coastal Meteorology Accelerated Research Initiative. Without the dedicated efforts of ETL staff, including S. Abbott, D. Gottas, J. Jordan, C. King, J. Leach, C. Russell, and others, the unique profiler and RASS data used here would not have been available. Jennifer Miletta (PMEL/JISAO) graciously provided the SSM/I data and interpretations, and we are grateful to Sarah Haines (University of North Carolina) for processing the aircraft data. The LAX profiler/RASS were operated by the South Coast Air Quality Management District (SCAQMD), and were provided by K. Durkee (SCAQMD). Access to a real-time data display system (the DARE workstation) supported by NOAA's Forecast Systems Laboratory aided research into this case. Nick Bond of the University of Washington/JISAO provided the digital data for the composite CTD used in Fig. 2. Substantive discussions with R. Rotunno, J. Klemp, and W. Skamarock of the National Center for Atmospheric Research concerning this event refined both the synoptic description and interpretations of the character of the perturbation. Reviews by Fred Sanders and an anonymous reviewer significantly improved the paper. Figures were expertly drafted by Jim Adams, and tables were prepared by Karen Martin.

REFERENCES

Bane, J. M., S. M. Haines, L. Armi, and M. H. Sessions, 1995: The California coastal marine layer: Winds and thermodynamics. June 1994 Aircraft Measurement Program Tech. Rep. CMS-95-1, 289 pp. [Available from University of North Carolina, Chapel Hill, NC 27599-3300.]

Banta, R. M., 1995: Sea breezes shallow and deep on the California coast. *Mon. Wea. Rev.*, **123,** 3614–3622.

Beardsley, R. C., C. E. Dorman, C. A. Friehe, L. K. Rosenfeld, and C. D. Winant, 1987: Local atmospheric forcing during the coastal ocean dynamics experiment. Part 1: A description of the marine boundary layer and atmospheric conditions over a northern California upwelling region. *J. Geophys. Res.*, **92,** 1467–1488.

Bluestein, H. B., 1986: Fronts and jetstreaks: A theoretical perspective. *Mesoscale Meteorology and Forecasting,* P. S. Ray, Ed., Amer. Meteor. Soc., 173–215.

Bond, N. A., C. F. Mass, and J. E. Overland, 1996: Coastally trapped wind reversals along the United States west coast during the warm season. Part I: Climatology and temporal evolution. *Mon. Wea. Rev.*, **124,** 430–445.

Brunt, D., and C. K. M. Douglas, 1928: The modification of the strophic balance for changing pressure distribution, and its effect on rainfall. *Mem. Roy. Meteor. Soc.*, **3,** 29–51.

Clark, J. H. E., and S. Dembek, 1991: The Catalina eddy event of July 1987: A coastally trapped mesoscale response to synoptic forcing. *Mon. Wea. Rev.*, **119,** 1714–1735.

Dorman, C. E., 1985: Evidence of Kelvin waves in California's marine layer and related eddy generation. *Mon. Wea. Rev.,* **113,** 827–839.

——, 1987: Possible role of gravity currents in northern California's coastal summer wind reversals. *J. Geophys. Res.*, **92,** 1497–1506.

——, L. Armi, J. M. Bane, and D. Rodgers, 1998: Sea surface mixed layer during the 10–11 June 1994 California coastally trapped event. *Mon. Wea. Rev.*, **126,** 600–619.

Ecklund, W. L., D. A. Carter, and B. B. Balsley, 1988: A UHF wind profiler for the boundary layer: Brief description and initial results. *J. Atmos. Oceanic Technol.*, **5,** 432–441.

Edinger, J. G., 1963: Modification of the marine boundary layer over coastal Southern California. *J. Appl. Meteor.*, **2,** 706–712.

Freeman, J. C., 1951: The solution of nonlinear meteorological problems by the method of characteristics. *Compendium of Meteorology,* T. Malone, Ed., Amer. Meteor. Soc., 421–433.

Gill, A. E., 1977: Coastally trapped waves in the atmosphere. *Quart. J. Roy. Meteor. Soc.*, **103,** 431–440.

——, 1982: *Atmosphere–Ocean Dynamics.* Academic Press, 662 pp.

Hermann, A. J., B. M. Hickey, C. F. Mass, and M. D. Albright, 1990: Orographically trapped coastal wind events in the Pacific Northwest and their oceanic response. *J. Geophys. Res.*, **95,** 13 169–13 193.

Joly, A., and A. J. Thorpe, 1990: Frontal instability generated by tropospheric potential vorticity anomalies. *Quart. J. Roy. Meteor. Soc.*, **116,** 525–560.

Klemp, J. B., R. Rotunno, and W. C. Skamarock, 1997: On the propagation of internal bores. *J. Fluid Mech.*, **331,** 81–106.

Leipper, D. F., 1995: Fog forecasting objectively in the California coastal area using LIBS. *Wea. Forecasting,* **10,** 741–762.

Mass, C. F., 1995: Comments on ''The dynamics of coastally trapped mesoscale ridges in the lower atmosphere.'' *J. Atmos. Sci.,* **52,** 2313–2318.

——, and M. D. Albright, 1987: Coastal southerlies and alongshore surges of the west coast of North America: Evidence of mesoscale topographically trapped response to synoptic forcing. *Mon. Wea. Rev.*, **115,** 1707–1738.

——, and ——, 1989: Origin of the Catalina eddy. *Mon. Wea. Rev.*, **117,** 2406–2436.

——, and N. A. Bond, 1996: Coastally trapped wind reversals along the United States west coast during the warm season. Part II: Synoptic evolution. *Mon. Wea. Rev.*, **124,** 446–461.

Maxworthy, T., 1983: Experiments on solitary internal Kelvin waves. *J. Fluid Mech.*, **129,** 365–383.

May, P. T., K. P. Moran, and R. G. Strauch, 1989: The accuracy of RASS temperature profiles. *J. Appl. Meteor.*, **28,** 1329–1335.

Miles, J., 1972: Kelvin waves on oceanic boundaries. *J. Fluid Mech.*, **55,** 113–137.

Miletta, J., 1993: Meteorological applications of coincident visible, infrared, and microwave observations from the Defense Meteorological Satellite Program. M.S. thesis, Dept. of Atmospheric Sciences, University of Washington, 86 pp. [Available from University of Washington, Seattle, WA 98195.]

National Research Council, 1992: *Coastal Meteorology: A Review of the State of the Science.* National Academy Press, 99 pp.

Neiburger, M., D. S. Johnson, and C. Chien, 1961: Studies of the structure of the atmosphere over the eastern Pacific Ocean in summer. Part I: The inversion over the eastern Pacific Ocean. *Univ. Calif. Publ. Meteor.*, **1,** 1–94.

Neiman, P. J., P. T. May, and M. A. Shapiro, 1992: Radio Acoustic Sounding System (RASS) and wind profiler observations of lower- and midtropospheric weather systems. *Mon. Wea. Rev.*, **120,** 2298–2313.

Nelson, C. S., 1977: Wind stress and wind stress curl over the California current. NOAA Tech. Rep. NMFS SSRF-714, 87 pp. [NTIS PB-273610.]

Nuss, W. A., and D. W. Titley, 1994: Use of multiquadric interpolation for meteorological objective analysis. *Mon. Wea. Rev.*, **122,** 1611–1631.

Persson, P. O. G., P. J. Neiman, and F. M. Ralph, 1995: Topographically generated potential vorticity anomalies: A proposed mechanism for initiating orographically trapped disturbances. Preprints, *Seventh Conf. on Mountain Meteorology,* Breckenridge, CO, Amer. Meteor. Soc., 216–222.

——, ——, and ——, 1996: The role of a topographically generated potential vorticity anomaly in initiating a coastal wind reversal. Preprints, *Conf. on Coastal Oceanic and Atmospheric Prediction,* Atlanta, GA, Amer. Meteor. Soc., 120–124.

Ralph, F. M., P. J. Neiman, D. W. van de Kamp, and D. C. Law, 1995: Using spectral moment data from NOAA's 404-MHz radar wind profilers to observe precipitation. *Bull. Amer. Meteor. Soc.*, **76,** 1717–1739.

Reason, C. J. C., and D. G. Steyn, 1992: The dynamics of coastally trapped mesoscale ridges in the lower atmosphere. *J. Atmos. Sci.*, **49,** 1677–1692.

——, and ——, 1995: Reply. *J. Atmos. Sci.*, **52,** 2319–2324.

Rogerson, A. M., and R. M. Samelson, 1995: Synoptic forcing of coastal-trapped disturbances in the marine atmospheric boundary layer. *J. Atmos. Sci.*, **52,** 2025–2040.

Samelson, R. M., 1992: Supercritical marine-layer flow along a smoothly varying coastaline. *J. Atmos. Sci.*, **49,** 1571–1584.

——, and A. M. Rogerson, 1996: Life cycle of a linear coastal-trapped disturbance. *Mon. Wea. Rev.*, **124,** 1853–1863.

Schär, C., and R. B. Smith, 1993: Shallow-water flow past isolated topography. Part I: Vorticity production and wake formation. *J. Atmos. Sci.*, **50,** 1373–1400.

Simpson, J. E., 1987: *Gravity Currents in the Environment and the Laboratory.* Ellis Horwood, 244 pp.

Skamarock, W. C., J. B. Klemp, and R. Rotunno, 1996: The diffraction of Kelvin waves and bores at coastal bends. *J. Atmos. Sci.*, **53,** 1327–1337.

Strauch, R. G., B. L. Weber, A. S. Frisch, C. G. Little, D. A. Merritt, K. P. Moran, and D. C. Welsh, 1987: The precision and relative accuracy of profiler wind measurements. *J. Atmos. Oceanic Technol.*, **4,** 563–571.

Thompson, W. T., T. Haack, J. D. Doyle, and S. D. Burk, 1997: A nonhydrostatic mesoscale simulation of the 10–11 June 1994 coastally trapped wind reversal. *Mon. Wea. Rev.*, **125,** 3211–3230.

Thorpe, A. J., H. Volkert, and D. Heimann, 1993: Potential vorticity of flow along the Alps. *J. Atmos. Sci.*, **50,** 1573–1590.

Weber, B. L., D. B. Wuertz, D. C. Welsh, and R. McPeek, 1993: Quality controls for profiler measurements of winds and RASS temperatures. *J. Atmos. Oceanic Technol.*, **10,** 452–464.

Whiteman, C. D., 1990: Observations of thermally developed wind systems in mountainous terrain. *Atmospheric Process over Complex Terrain, Meteor. Monogr.*, No. 45, Amer. Meteor. Soc., 5–42.

Wilczak, J. M., and Coauthors, 1995: Contamination of wind profiler data by migrating birds: Characteristics of corrupted data and potential solutions. *J. Atmos. Oceanic Technol.*, **12,** 449–467.

Winant, C. D., C. E. Dorman, C. A. Friehe, and R. C. Beardsley, 1988: The marine layer off northern California: An example of supercritical channel flow. *J. Atmos. Sci.*, **45,** 3588–3605.